

Ultrasound Based Botanical Extraction Unit

The Potential of an Ultrasonic Phased Array System in Botanical Extraction



Presented by:
Marion Boynton

Prepared for:
J. Son
Dept. of Electrical and Electronics Engineering
University of Cape Town

Submitted to the Department of Electrical Engineering at the University of Cape Town in
partial fulfilment of the academic requirements for a Bachelor of Science degree in
Mechatronics

October 14, 2019

Declaration

1. I know that plagiarism is wrong. Plagiarism is to use another's work and pretend that it is one's own.
2. I have used the IEEE convention for citation and referencing. Each contribution to, and quotation in, this report from the work(s) of other people has been attributed, and has been cited and referenced.
3. This report is my own work.
4. I have not allowed, and will not allow, anyone to copy my work with the intention of passing it off as their own work or part thereof.

Signature: 
Marion Boynton

Date: 14/10/2019

Acknowledgments

I would like to thank my supervisor, Jarryd Son, for his time and effort in helping me to complete this project.

I would like to thank Dr Amit Mishra for his time and advice.

I would like to thank Dr Andrew Wilkinson for sharing his transmitters and receivers with me as well as some of his vast knowledge in the field of ultrasound.

Lastly, to my parents, who have provided me with an immense amount of love and support throughout my studies.

Abstract

There is a current need to design more effective systems for botanical extraction. This report investigates the potential of ultrasonic phased array technology in the extraction of botanical compounds from plants. Ultrasound is currently used in plant extraction but there is a need for improvement on ultrasonic extraction system designs as current systems are limited to small volumes and consume high power.

The project involves the implementation of an airborne ultrasonic phased array system as well as a simulation software. The physical system and simulation tool are used to analyse ultrasonic phased array systems. This investigation confirms the effectiveness of phased array systems and further explores how such systems could be successful in ultrasonic botanical extraction.

Contents

1	Introduction	1
1.1	Background to the study	1
1.2	Objectives of this study	1
1.2.1	Problems to be investigated	2
1.2.2	Purpose of the study	2
1.3	Scope and Limitations	2
1.4	Plan of development	3
2	Literature Review	5
2.1	Ultrasonic Botanical Extraction	5
2.1.1	Instrumentation used in UAE	7
2.2	Basics of Ultrasound Waves	9
2.2.1	Ultrasonic Transducers	10
2.2.2	Ultrasonic Wave Propagation	10
2.3	Ultrasonic Phased Arrays	13

2.3.1	Principles of Phased Array Technology	13
2.3.2	Developments in Ultrasonic Phased Array Technology	13
3	Design	15
3.1	Selection of Transducers	15
3.2	Driving Electronics and Signal Generation	16
3.3	Setup Design	20
4	Implementation	23
4.1	Experimental Preparation	23
4.1.1	Polarity Test	23
4.2	Testing	24
4.3	Simulations	29
5	Results	31
6	Discussion	38
7	Conclusions	41
8	Recommendations	42
A		45
A.1	MATLAB and Arduino Code	45
A.2	MATLAB simulations of beam patterns for Tests 1 - 4	45

B	47
B.1 Tables of Experimental Results	47
C	55
C.1 PDFs for lasercutting parts for testing stand	55

List of Figures

2.1	The cavitation process - the bubble forms, grows and undergoes implosive collapse .[?]	6
2.2	Diagrams of the two ultrasonic extraction systems currently used[?]	8
2.3	The Acoustic Spectrum. The ultrasonic range of frequencies can be subdivided into three sections as shown.[1]	9
2.4	Propagation of an Acoustic Wave in a homogeneous medium where C is the compression and D is the decompression of the medium's particles.[2]	11
2.5	The Inverse Square Law for an acoustic wave. As the wave propagates, the beam diverges over a greater area proportional to the square of the distance travelled. The intensity therefore decreases proportionally to the inverse of the square of the distance travelled[?]	12
3.1	Pin-out diagram of the Arduino Mega 2560 [3]	17
3.2	Two square wave signals generated at the pins of the Arduino. The first wave has no applied delay and the second has a delay of $3.55 \mu s$	19
3.3	Voltage signals measured across two transmitters when supplied with the signals in Figure 3.2 amplified to 20 Vpp by a L298N Dual H-Bridge Motor Driver.	20
3.4	Configurations of transmitters and receivers for testing	20
3.5	Coordinate systems used for measurements, plots of results and simulations	22

4.1	Polarity Test	24
4.2	Experimental Setup	25
4.3	Oscilloscope probe measuring the voltage across a receiver	25
4.4	Signal generated across a receiver when placed opposite multiple emitting transmitters.	26
4.5	Signal generated across a receiver when placed opposite multiple emitting transmitters with timescale scaled up to 2 ms per division.	26
4.6	Signal generated across a receiver when placed opposite multiple emitting transmitters with timescale scaled up to 50 ms per division.	26
4.7	Timing diagram for the signals to be applied to the 7 transducers to focus at $F = [0.018 \ 0 \ 0.05] \text{ m}$	28
4.8	Signals generated at A7 and C1 (or D29 and D36 as labelled on the Arduino Mega 2560). The signal generated at A7 has no delay and the signal at C1 is at a delay of $7.65 \mu\text{s}$	28
4.9	Timing diagram for the signals to be applied to the 7 transducers to focus at $F = [0 \ 0.018 \ 0.05] \text{ m}$	29
5.1	Plot of the voltage readings of the acoustic field produced by the circular array of transmitters when no delays are implemented.	32
5.2	Simulation of the acoustic pressure field produced by the circular array of transmitters when emitting in phase	32
5.3	Plot of the voltage readings of the acoustic field produced by the circular array of transmitters when a delay is applied to focus the beam at $F = [0 \ 0 \ 0.05] \text{ m}$	33
5.4	Simulation of the acoustic pressure field produced by the circular array of transmitters when a delay is applied to focus the beam at $F = [0 \ 0 \ 0.05] \text{ m}$	33
5.5	Plot of the voltage readings of the acoustic field produced by the circular array of transmitters when a delay is applied to focus the beam at $F = [0.018 \ 0 \ 0.05] \text{ m}$	34

5.6	Simulation of the acoustic pressure field produced by the circular array of transmitters when a delay is applied to focus the beam at $F = [0.018 \ 0 \ 0.05]$ m	35
5.7	Plot of the voltage readings of the acoustic field produced by the circular array of transmitters when a delay is applied to focus the beam at $F = [0 \ 0.018 \ 0.05]$ m	35
5.8	Simulation of the acoustic pressure field produced by the circular array of transmitters when a delay is applied to focus the beam at $F = [0.018 \ 0 \ 0.05]$ m	36
5.9	Plot of the voltage readings of the acoustic field produced by the capped sphere of transmitters	37
5.10	Simulation of the acoustic pressure field produced by the capped sphere of transmitters	37
6.1	The flat, circular array of transmitters with arrow 1 and arrow 2 indicating the approximate positions of the focal points on the x-y plane for Test 4 and Test 3 respectively	39
A.1	Beam Patterns Simulated for Different Tests	46

List of Tables

3.1	Truth Tables for the operation of Motor A and Motor B of the L298N Dual H-Bridge Motor Driver.[4]	19
B.1	Results for the tests done with the linear flat array with no delays implemented (no delays) and focusing at $F = [0 \ 0 \ 0.05]$ (z focus)	47
B.2	Results for the tests done when focusing at $F = [0.018 \ 0 \ 0.05]$ (titled x focus) and $F = [0 \ 0.018 \ 0.05]$ (titled y focus) and for the capped sphere array.	52

Chapter 1

Introduction

1.1 Background to the study

Over the past several years there has been a significant rise in interest in the potential of plants in many industries. Many plant compounds that have valuable properties have been discovered and there are likely many more still to be found. These compounds can be used in many different applications such as pharmaceuticals, agriculture, food processing and beauty products.

There are many methods used to extract these compounds from botanicals. Different methods are used for the extraction of different compounds depending on the requirements for the product. Solvents are often used such as alcohol and water to diffuse the plant matter and draw out the compounds. Harsher chemicals are also sometimes used as solvents for compounds that are more difficult to reach but since the residue of the solvent is difficult to completely eliminate, these chemicals are not suitable for the extraction of compounds that will be ingested by humans.

1.2 Objectives of this study

The objectives of this project are:

- Design and build an ultrasonic phased array system that could be developed for use in

1.3. SCOPE AND LIMITATIONS

ultrasonic botanical extraction

- Test the effectiveness of the system at generating regions of high intensity
- Analyse the results from testing and arrive at conclusions
- Provide recommendations that can improve on this project and how this project can be developed for future work potential

1.2.1 Problems to be investigated

The problem to be investigated is whether an ultrasonic phased array system could be used effectively in ultrasonic botanical extraction.

1.2.2 Purpose of the study

There is a rapidly growing market for plant based solutions in a wide range of fields. Most notably, botanical extracts can be used in treatments for cancer and other illnesses as well as in nutritional supplements and added to foods, beverages and products to provide numerous health benefits. Plant extracts can also be used in industrial processes and given the increasing environment concerns around non natural processes one can expect increasing focus on naturally sourced raw materials. Therefore the development of an economically feasible, high quality yield, botanical extraction unit would help to make powerful plant extracts more available to people from all backgrounds - rich and poor and would clearly serve a growing need.

1.3 Scope and Limitations

The initial scope of this project was to explore the potential of ultrasonic phased array systems in botanical extraction. The scope can be factored into the following:

- Assembling an array of ultrasonic transducers to transmit airborne ultrasound waves. No immersible or waterproof transducers were used.
- The transducers used were rated 40 kHz and the signals used to drive them were generated at 40 kHz. Transducers with different resonant frequencies were not investigated.

1.4. PLAN OF DEVELOPMENT

- The signals fed to drive the transmitters were generated using an Arduino Mega 2560 as well as amplifying circuitry. Other microcontrollers and integrated circuits, such as a Field Programmable Gate Array (FPGA), were not investigated.
- Designing and building a structure to test the effectiveness of the phased array system at generating different regions of high intensity.

The project was limited to a duration of 12 weeks and a budget of R1500. These limitations restricted the components choice to affordable and easily available components. The project was thus limited to airborne ultrasound. This prevented the project from developing a botanical extraction unit that can produce ultrasound fields in a solution of plant matter.

The time and budget restrictions also limited the accuracy of the results measurements.

1.4 Plan of development

The report has been divided into several chapters following the project implementation process. It begins with a review of the literature read during the research stage of the project. The principles of ultrasonic botanical extraction, ultrasound waves and phased array systems are explained. Developments of systems in these fields are also reviewed.

The design process of the system is then elaborated on. This is broken down into three stages:

1. Transducer Selection
2. Driving Electronics.
3. Setup Design

The report then details the implementation process including the testing procedure and the development of a simulation program.

Following this the results are displayed as both as plots of the experimental results and as plots of simulations of the ideal expected results.

A discussion chapter is then included that comments on the results and compares the experimental results to the simulations.

1.4. PLAN OF DEVELOPMENT

A conclusion chapter follows. The project investigation and the findings of the project is brought together.

The final chapter provides recommendations to those who may want to implement a similar project. Areas that should be further explored are recommended. A final discussion on possible future developments in this area is included.

Chapter 2

Literature Review

Extensive research was carried out in order to understand the workings of ultrasonic botanical extraction and ultrasonic phased arrays. This section will lay out the theory covered during this research stage as well as look into technological developments in both areas. It will begin by covering the basics of ultrasonic botanical extraction and analyse the current methods. It will then go into the fundamentals of ultrasound waves. Finally, phased array systems will be explained and technological developments using phased arrays will be investigated.

2.1 Ultrasonic Botanical Extraction

There are currently several different methods of extracting plant compounds. Conventional methods, such as Soxhlet extraction, maceration, infusion and solid-liquid extraction (SLE) [5], are long processes and often use toxic solvents to rupture the plant cell walls. These methods are being phased out by newer extraction technologies that improve both the final extract quality and the extraction process significantly. Some of the more recent extraction methods are Ultrasound-assisted extraction(UAE), microwave-assisted extraction (MWE), sub-critical and supercritical fluid extraction (SFE) and enzyme assisted extraction.[5]

UAE has emerged over the past several years as a highly effective method for botanical extraction. UAE involves transmitting ultrasound waves into a solution of plant parts, such as stems, leaves and roots, immersed in a solvent. This solution is known as a plant slurry or plant solution. Ultrasound waves are longitudinal, pressure waves that require a medium through which to travel. When they propagate through a medium the molecular structure of the medium is exposed to alternating high-pressure (compression) and low-pressure (rarefaction) cycles.[6]

2.1. ULTRASONIC BOTANICAL EXTRACTION

Molecules are pushed together during compression and pulled apart during expansion.

In a liquid medium, if the ultrasound intensity is high enough, the expansion cycle can produce microscopic dissolved gas bubbles in the solution. The bubbles grow and undergo implosive collapse under the influence of the ultrasonic field. The process of the formation, growth and collapse of the micro-bubbles is termed “cavitation”. The cavitation process is depicted in Figure 2.1. If cavitation occurs due to ultrasound waves propagating through the liquid medium, it is termed acoustic cavitation. The implosive collapse of the bubbles during cavitation generates very high pressures and temperatures as well as shear forces and turbulence which break the plant cell walls and results in the release of botanical compounds.

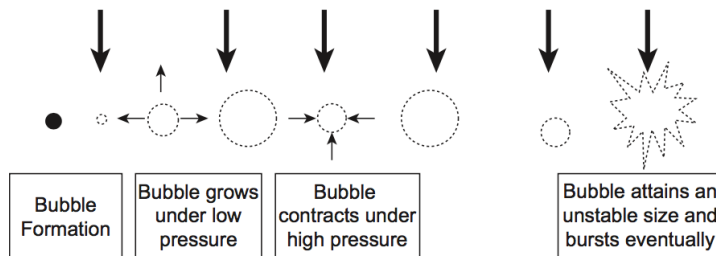


Figure 2.1: The cavitation process - the bubble forms, grows and undergoes implosive collapse .[?]

There are other extraction methods that are also based on the process of cavitation, namely, negative pressure cavitation (NPC) extraction and hydrodynamic cavitation extraction (HCE).[5] These methods generate cavitation through hydrodynamic principles instead of ultrasound. Cavitation-based extraction (CE) methods pose many advantages over conventional extraction methods including a greater extraction yield of higher quality and purity, reduced extraction time, reduced energy consumption and reduced solvent consumption.[5] These factors result in CE methods being considerably more environmentally friendly processes than conventional extraction methods.

Another significant advantage is the elimination of the use of toxic solvents in the extraction process. Conventional extraction methods often use toxic solvents, which result in residues in the final extract that are difficult to completely get rid of. CE methods can effectively extract plant compounds without using toxic solvents. The quality of the extract can also be degraded due to high temperature exposure in conventional methods, which affects heat sensitive compounds in the plant extract.[5]

UAE and other CE methods provide numerous benefits and have great potential to advance botanical extraction technologies. However, there are some concerns. UAE does not produce uniform cavitation activity within the solution as the ultrasound intensity decreases rapidly at small distances from the source. UAE also requires a significant amount of energy compared

to alternative methods, such as NPC.[5]

2.1.1 Instrumentation used in UAE

An ultrasonic botanical extraction system consists of a generator and a transducer. The generator supplies the required electric signal. The transducer is a device that converts the electrical energy into a mechanical vibration. The transducer is made of piezoelectric crystals, which are crystals that produce a mechanical vibration in response to an electric signal. When an electric signal of a frequency in the ultrasonic range (greater than 20 kHz) is transferred to a transducer, the transducer will vibrate and produce pressure waves of the same frequency in the medium that it is exposed to.

There are currently two ultrasonic extraction systems, , also known as an ultrasonic extractors or sonochemical reactors, used for botanical extraction. A probe system, as shown in Figure 2.2a, and an ultrasonic bath, as shown in Figure 2.2b.

Ultrasonic Probe Extraction System

A probe system consists of an ultrasonic electric generator, a transducer and a probe. The generator generates an electrical signal of high frequency that is used to power the transducer. The transducer converts the electrical signal into a mechanical vibration, which is transferred to the probe, which expands and contracts longitudinally. The vibration is amplified and transmitted down the length of the probe. The probe is in contact with the solution so the energy is transmitted to the solution resulting in acoustic cavitation.

The ultrasonic probe system is a direct form of sonication meaning that the part vibrating and producing the ultrasound (in this case the probe) is in direct contact with the plant solution.

The probe method of sonication has the advantage of transmitting high intensity acoustic energy but it is limited to a small region. It is therefore ineffective for larger process volumes. The probe tip also erodes over time due to the cavitation and therefore must be replaced. Probe type systems are therefore usually only used for experiments at a laboratory scale and exploratory studies.[6]

2.1. ULTRASONIC BOTANICAL EXTRACTION

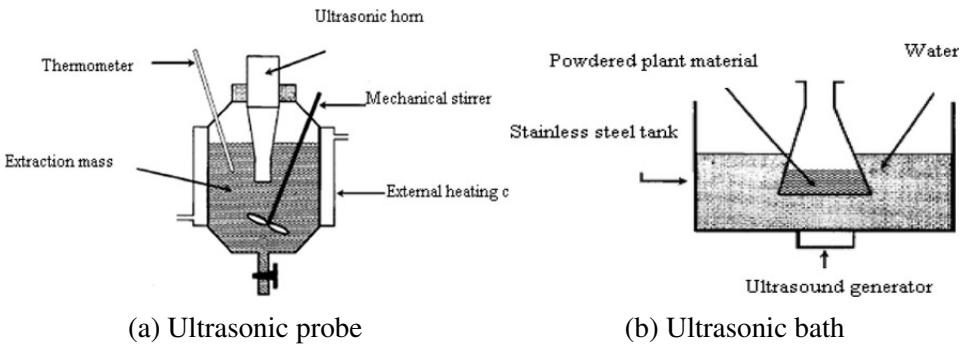


Figure 2.2: Diagrams of the two ultrasonic extraction systems currently used[?]

Ultrasonic Bath Extraction System

Ultrasonic baths have the transducers attached to the bottom or sides of a stainless steel tub thus the whole tub vibrates and transmits the ultrasonic energy to the liquid inside it. A single transducer or multiple transducers can be used. The ultrasonic bath can implement indirect sonication by placing the plant solution in a separate vessel within the bath, as in Figure 2.2b, or it can implement direct sonication by placing the plant solution directly in the bath.

The ultrasonic bath has the advantage of producing an evenly distributed acoustic field throughout the liquid medium.[6] It is also generally more easily available and cost effective relative to the process volume than the probe system. The bath system does however dissipate less power from the bath into the solution than a probe system.

Design Considerations for Ultrasonic Extraction Systems

Gogate and Patil note that there is a need for the design of new reactors that are more efficient, cost-effective and consume less power.[7] They give advice on designing effective ultrasonic extractors for future work.[?] Their main points can be summarized as:

- More transducers tend to produce more uniform cavitation within the reactor vessel, which is desirable.
- The geometric configuration of the reactor should be optimized to obtain uniform cavitation activity distribution in the reactor.[7]
- The number and location of the transducers must be carefully considered.
- Simulations of the resulting sound pressure fields should be implemented and used to optimize designs.[8] The simulations should be used to analyse the effects of different

operating and geometric parameters.

Using multiple transducers in designs has several benefits. Firstly, the use of multiple transducers allows individual transducers to dissipate lower power while maintaining the required overall power dissipation levels in the reactor.[6] Another significant advantage is being able to arrange them to generate a uniform acoustic field.[7] Using multiple transducers also allows one to use multiple frequencies in the sonication process, which can be beneficial for the extraction of certain compounds.

2.2 Basics of Ultrasound Waves

Ultrasound waves are sound waves, or acoustic waves, with frequencies in the ultrasonic range, which is beyond the human hearing range of frequencies. Sound can be divided into three ranges of frequencies as shown in Figure 2.3. Ultrasound waves have frequencies above 20 kHz. The frequencies used in ultrasonic botanical extraction are in the low frequency range, usually between 20 and 40 kHz.

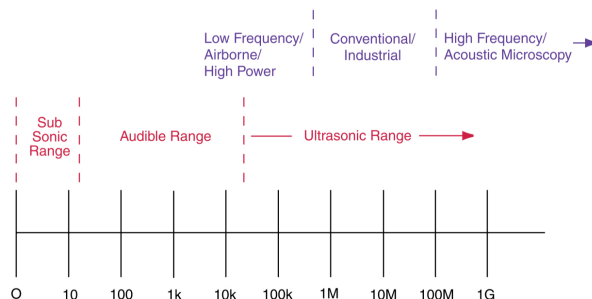


Figure 2.3: The Acoustic Spectrum. The ultrasonic range of frequencies can be subdivided into three sections as shown.[1]

Acoustic waves travel by pressure variations. They therefore require a medium to travel through as they alternately expand and contract the medium's particles as they propagate.[2] Acoustic waves are produced by mechanical vibrations that cause the pressure variations to occur. The frequency of an acoustic wave corresponds to the frequency of the mechanical vibration causing it. Ultrasound waves are therefore generated by mechanical vibrations at ultrasonic frequencies. These vibrations can be produced by ultrasonic transducers.

2.2.1 Ultrasonic Transducers

Ultrasonic transducers are devices that convert an electric signal into a mechanical vibration or conversely, a mechanical vibration into an electric signal. They work on the basis of the piezoelectric effect, which is a property shown by some materials known as piezoelectric crystals. The piezoelectric effect is the generation of a voltage due to mechanical deformation. The reciprocal piezoelectric effect can be used to convert electrical energy into mechanical energy. An alternating voltage applied to a piezoelectric crystal results in a mechanical oscillation at the same frequency as that of the voltage signal supplied. Maximum oscillation occurs at resonance when the electric signal applied is at the natural frequency of the piezoelectric crystal.

2.2.2 Ultrasonic Wave Propagation

The velocity of sound is the rate at which the vibratory energy is transmitted in the direction of propagation.[9] The velocity, v , of a sound wave, and all waves, is the product of its frequency, f , and wavelength, λ :

$$v = \lambda f \quad (2.1)$$

Velocity is a vector quantity consisting of a magnitude and direction. Speed is the magnitude of the sound velocity. The speed of sound, c , through a particular medium depends on the density and elasticity of the medium:

$$c = \frac{\kappa}{\rho} \quad (2.2)$$

where ρ is the density of the medium and κ is the elastic modulus of the medium, which is a measure of the medium's resistance to compression.[10] The speed of sound in air is about 343 m/s and about 1 500 m/s in water.

Acoustic waves can be represented as a sine wave where the wave's amplitude is the maximum change in the medium's pressure caused by the vibration. This is shown in Figure 2.4 below.

The acoustic wave equation is given as:

$$\nabla^2 p = \frac{1}{c^2} \frac{\partial^2 p}{\partial t^2} \quad (2.3)$$

where p is the pressure of the wave, c is the speed of sound in the particular medium, and t is the time.[10] From this, an expression for the pressure wave can be derived. The pressure due

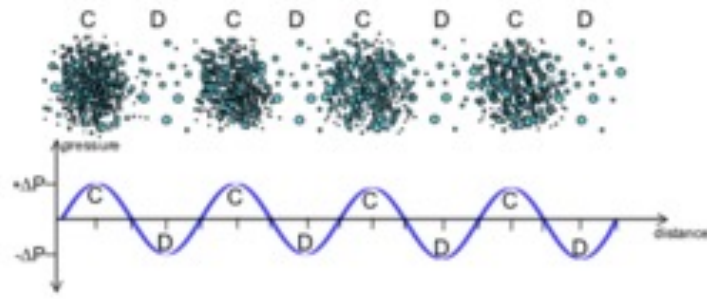


Figure 2.4: Propagation of an Acoustic Wave in a homogeneous medium where C is the compression and D is the decompression of the medium's particles.[2]

to a single, omnidirectional acoustic source at a distance, r , from the source is:

$$pr, t = \frac{A}{r} \cos kr - \omega t - \delta \quad (2.4)$$

where A is the amplitude of the wave, ω is the angular frequency,

$$k = \frac{\omega}{c}$$

is the wavenumber and δ is the initial phase of the wave (the delay).[10]

The intensity, I , at a point is the amount of energy, or power, P , passing perpendicularly through a unit cross-sectional area, A , per unit time at that point.[11]

$$I = \frac{P}{A} \quad (2.5)$$

The intensity of an acoustic wave is proportional to the square of the amplitude of the pressure wave. The relationship is equated as:

$$I = \frac{\Delta p^2}{2\rho c} \quad (2.6)$$

where Δp is the pressure variation or amplitude of the acoustic pressure wave measured in Pascals (Pa) or N/m^2 , ρ is the density of the medium of propagation and c is the speed of sound in the medium.

As a sound wave propagates, the intensity decreases with the distance travelled. This phenomenon is termed acoustic attenuation. Acoustic attenuation is mainly due to two factors.

The first reason for acoustic attenuation is beam spreading, which occurs as a result of the divergence of the ultrasound beam.[10] The wave from a point source of spherical radiation

2.2. BASICS OF ULTRASOUND WAVES

experiences a decrease in intensity due to beam spreading proportional to the inverse of the square of the distance from the source. This is because as the wave propagates from the source, its energy is being spread over an increasingly larger, spherical surface area. Since the surface area of a sphere increases proportionally to the square of its radius, the intensity decreases proportionally to the inverse of the square of the distance travelled. This is known as the inverse square law.[12] The pressure amplitude experiences a decrease proportional to the inverse of the distance travelled from the source as intensity is proportional to the square of the pressure.

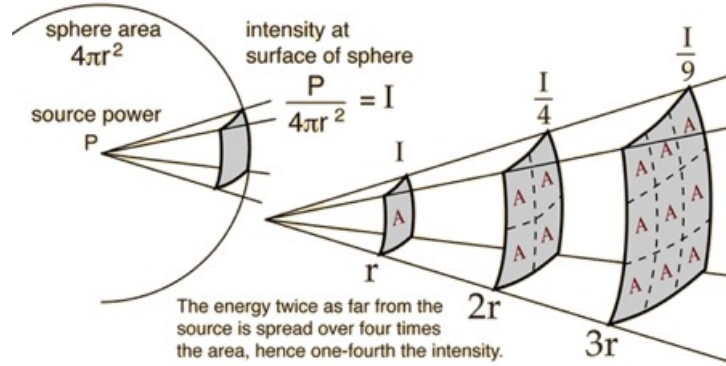


Figure 2.5: The Inverse Square Law for an acoustic wave. As the wave propagates, the beam diverges over a greater area proportional to the square of the distance travelled. The intensity therefore decreases proportionally to the inverse of the square of the distance travelled[?]

The second reason a wave decreases in intensity as it propagates is that the medium of propagation absorbs some of the wave energy as it passes through. The decrease in the pressure wave amplitude due to absorption can be represented as a function of the distance travelled, x , and the absorption coefficient, α , which is dependent on the wave frequency and the medium of propagation:

$$A = A_0 e^{-\alpha x} \quad (2.7)$$

where A_0 is the initial wave amplitude.

Since intensity is proportional to the square of the pressure wave amplitude, the decrease in intensity due to absorption is:

$$I = I_0 e^{-2\alpha x} \quad (2.8)$$

The absorption coefficient increases with increasing frequency.[11] The absorption coefficient depends on various properties of the medium such as temperature, density and pressure.[12] Absorption coefficients for sound waves is greater in less dense, gaseous mediums such as air than in liquids and solids where the acoustic wave travels faster and less of the energy is absorbed.

The effect of absorption for ultrasonic waves in the lower frequency range (20 kHz - 100 kHz) when propagating through liquid mediums is relatively small. This is why sonar is so effective.[13]

For botanical extraction, low ultrasonic frequencies (usually between 25 and 40 kHz) are transmitted through liquids over small distances (usually less than a metre). The attenuation due to absorption in ultrasonic botanical extraction is generally negligible. Ultrasound waves of low frequencies transmitted through air have a much larger absorption coefficient and will attenuate the wave amplitude considerably when the ultrasound is transmitted at distances over a metre.

2.3 Ultrasonic Phased Arrays

2.3.1 Principles of Phased Array Technology

A phased array system is a collection of emitting elements where the signals feeding each element are at specific relative phases. The phases are calculated so that the wave interference pattern resulting from the multiple sources has a specific region of high intensity. This is due to the waves' constructive interference and the region is termed the main lobe. The direction and shape of the main lobe can be dynamically manipulated by applying different phases to each element's feeding signal.

Phased array systems are used in a range of applications with different types of waves.

Single-element ultrasonic probes emit a beam in a fixed direction and therefore must be mechanically steered to reach a larger region. Phased array technology allows the beam to be focused and steered electronically at exact focal distances and angles. Phased array technology is extremely flexible in its ability to effectively control the beam and the ultrasound field properties. It has several other advantages including that it requires less mechanical parts, less maintenance and is more accurate due to less human involvement as it is electronic.

2.3.2 Developments in Ultrasonic Phased Array Technology

Ultrasonic phased arrays are widely used in many different fields. Most notably, it is used in medical ultrasound imaging as well as for advanced Non-Destructive Testing (NDT) of

2.3. ULTRASONIC PHASED ARRAYS

materials in industries such as nuclear, aeronautic and in-line testing.[14]

Ultrasonic phased arrays have been effectively used in wireless power transfer (WPT).[15] Power can be transferred more efficiently by focusing the acoustic waves to receivers at different locations.

Marzo *et al.* have developed a phased-array system for narrowband airborne ultrasound transmission called ‘Ultraino’. [16] Ultraino is an open platform designed to be flexible, inexpensive and easily implementable for use in research and exploration. The software allows one to set the geometric configuration of an array of transducers and simulate the resulting acoustic field in real time. Several examples of possible applications for Ultraino are provided including a parametric loudspeaker, an acoustic levitator and for haptic feedback. Details on how to assemble a phased array for each of these applications is provided in the report [16] and its Supplementary Movies. The Ultraino software is used to electronically steer the focal point of the acoustic field produced by the arrays by altering the phase delays for signals applied to each transducer.

The Ultraino projects use inexpensive, widely available, 40 kHz ultrasonic transmitters and an Arduino Mega and amplifying circuitry to drive them. 64 digital signals can be generated with the Arduino Mega and the signal properties can be defined in code. As an open platform, Ultraino has opened up the doors to many people to explore the possibilities of phased array systems.

‘UltraHaptics’ is another system designed with a phased array of 40 kHz ultrasonic transmitters.[17] This system focuses the emitted ultrasound at different points in space where it produces haptic feedback. The focused ultrasound stimulates receptors in the human body resulting in tactile sensations. Haptic feedback has potential in numerous applications such as improving the AR and VR experiences, replacing the controls in driving and the interfaces for machines such as ATMs.

Chapter 3

Design

After carrying out extensive research into the process of ultrasonic botanical extraction and the physics of ultrasound and phased arrays, an experiment needed to be designed to verify the effectiveness of ultrasonic phased array systems in producing regions of high intensity. If such a system was implemented in a liquid medium, the regions of high intensity would result in acoustic cavitation, as required for ultrasound botanical extraction. The ultimate objective would be the effective extraction of plant botanicals from a plant slurry solution.

The design was done in two stages. Firstly, the components for the experiment were selected. The transducers were chosen first as they are the most critical part in the system. Then, the components to drive the transducers were selected and the driving signals were generated. Finally, the full experiment was designed based on the components.

3.1 Selection of Transducers

It was vital that the transducers were selected before any other component or design choices could be made. This is because there is a wide range of transducers available used for many different applications. They exist in many different shapes and sizes with different power consumption, rated frequencies, optimal voltages and are manufactured for different environmental conditions. They also vary greatly in price.

Several types of transducers were considered. Ideally the transducers used for this project would have been immersible in liquids so that botanical extraction could be implemented. However, commercially available, immersible transducers are expensive and generally large

3.2. DRIVING ELECTRONICS AND SIGNAL GENERATION

so require high power driving electronics. The project budget did not permit acquisition of this equipment and so the project was amended to explore the potential of phased array systems to create the conditions likely to be necessary for ultrasonic botanical extraction. The testing was therefore done using air as a transmission medium and low cost non immersible transducers that are simple to power.

Low cost, ultrasonic transducers are widely available for use as proximity sensors. These transducers are sold both as transmitters and receivers. They both consist of a small piezoelectric crystal inside a protective casing; however they are designed slightly differently for different functions. The transmitter is designed to be at its minimum impedance at its rated (resonant) frequency whereas the receiver is designed to be at its maximum impedance at its rated frequency. This allows the transmitter to be driven at maximum power when supplied with a signal of the rated frequency and the receiver to generate maximum voltage when sensing a signal of the rated frequency.[18]

It was decided that several of these transmitters would be suitable to form an airborne ultrasonic phased array. This design choice was supported by several reports on ultrasonic phased array systems.[16][17]

The transmitters selected were Kobitone, 40KHZ, 255-400ST16-ROX transmitters and the receivers were 40 kHz, TCT40-16R receivers. These were chosen as they were available through UCT at a reduced price due to them being used for a phased array project for the course, EEE3097S. Similar transmitters and receivers with the same specifications are widely available.

3.2 Driving Electronics and Signal Generation

The transducers had to be powered to produce acoustic waves of desired phase and amplitude. The transducers chosen have a resonant frequency of 40 kHz and an optimal voltage of 20 V. Powering a transducer with a signal at its resonant frequency ensures the majority of the energy in the input signal is transferred to the transducer's output signal. A square wave was used to power the transducers as it can deliver more power than a sine wave of the same amplitude. Therefore 40 kHz square waves had to be generated.

An Arduino Mega 2560 was used to generate the square wave signals at specific phases as it has many digital output pins, is affordable and information on how to code in the Arduino IDE is widely available. The Arduino Mega has 54 digital Input/Output pins and 16 analog input

3.2. DRIVING ELECTRONICS AND SIGNAL GENERATION

pins. These pins are divided into 8 8-bit ports, Port A-F. The pin-out for the Arduino Mega 2560 that was used as a reference in writing the code is shown in Figure 3.1.

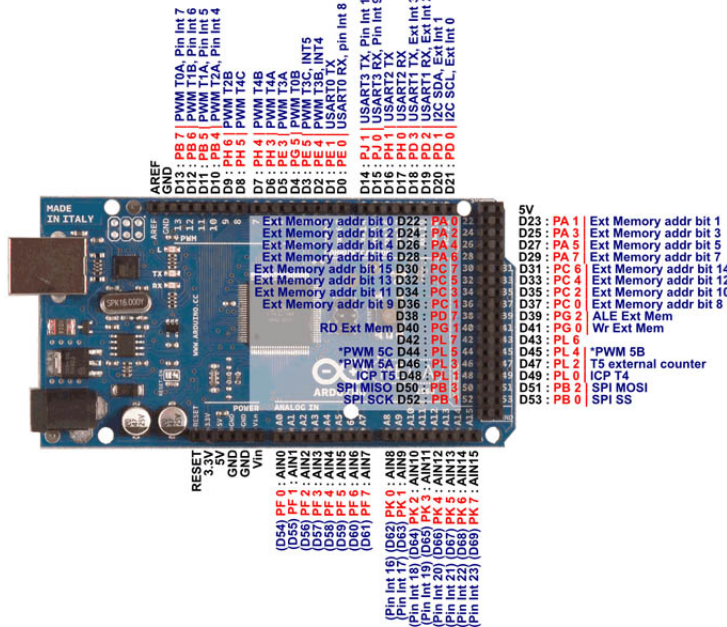


Figure 3.1: Pin-out diagram of the Arduino Mega 2560 [3]

The ports were directly manipulated in the code to allow the pins to be turned on and off rapidly (in the order of nanoseconds) and simultaneously. The period of a 40 kHz signal is $25 \mu s$, ($T = \frac{1}{f}$) therefore a pin must be held high for $12.5 \mu s$ and low for $12.5 \mu s$ within each cycle.

A function `_delay_us(float)` was found in the Arduino AVR library that applies the specified delay in μs as the corresponding number of clock cycles of the Arduino's CPU. Since this function takes floating point numbers, very accurate timing can be implemented as required.

The phase differences between signals were achieved by applying a time delay between the onset of different pins from 0 to 1 and 1 to 0. The code to generate a 40 kHz square waves at Port A, C and L with the pins of Port C at a delay of $8.7 \mu s$ is included in 3.2. The other delay sequences implemented as Arduino Code is included in the GitHub repository. A link to this is included in Appendix A.

Listing 3.1: Arduino code example

```
#include <util/delay.h>

void setup() {
    DDRA = 0b11111111; // outputs
    DDRC = 0b11111111;
    DDRL = 0b11111111;
}
```

3.2. DRIVING ELECTRONICS AND SIGNAL GENERATION

```
void loop() {
    noInterrupts();
    PORTA = 0b10101010;
    PORTL = 0b10101010;
    PORTC = 0b01010101;
    _delay_us(8.62);
    PORTC = 0b10101010;
    _delay_us(3.5);

    PORTA = 0b01010101;
    PORTL = 0b01010101;
    _delay_us(8.62);
    PORTC = 0b01010101;
    _delay_us(3.5);
    interrupts();
}
```

Each port has three registers that define properties of the pins. The DDR register sets the pins to inputs (if the pin's bit is set to 0) or outputs (if the pin's bit is set to 1). The PORT register sets the pins HIGH (1) or LOW (0). The PIN register reads the state of the input pins.[19]

The three lines in the setup set all the pins in the ports A, C and L as outputs. The line 'PORTA = 0b10101010' from the loop sets the pins of Port A as HIGH if set to 1 or LOW if set to 0.

The *_delay_us(float)* lines of code hold the pins in their current state for the specified time in μs . This is how the desired square waves are generated.

Since Arduino pins are limited to 5 V pp, the signals were amplified to obtain an input signal of the transmitters' optimal voltage (20 Vpp). The L298N Dual H-Bridge Motor Driver was chosen to amplify the signals. This Dual H-Bridge driver takes a power supply of 5 to 35 V and can amplify the voltage up to 46 V. The ENA and ENB pins are set to HIGH to turn the motors on and the direction of the motors are controlled by IN1 and IN2 for Motor A and IN3 and IN4 for Motor B. A truth table for the operation of the motor driver is shown in Table 3.1.

When a square wave is supplied to IN1 and the inverse of that wave to IN2 the motor driver is constantly alternating. Every second pin of the Arduino was set to the inverse of the previous so that a pair of inverse square wave signals could be used as two motor driver inputs (IN1 and IN2 or IN3 and IN4). These inputs therefore constantly alternate between 1 and 0 at a set rate

3.2. DRIVING ELECTRONICS AND SIGNAL GENERATION

Table 3.1: Truth Tables for the operation of Motor A and Motor B of the L298N Dual H-Bridge Motor Driver.[4]

ENA	IN1	IN2	State
0	N/A	N/A	Motor A off
1	0	0	Motor A is stopped (brakes)
1	0	1	Motor A is on and turning backwards
1	1	0	Motor A is on and turning forwards
1	1	1	Motor A is stopped (brakes)

ENB	IN3	IN4	State
0	N/A	N/A	Motor B off
1	0	0	Motor B is stopped (brakes)
1	0	1	Motor B is on and turning backwards
1	1	0	Motor B is on and turning forwards
1	1	1	Motor B is stopped (brakes)

(the frequency of the signals) and are always the opposite state to one another. The direction of the output current from the motor driver is alternated between the two output pins of the motor driver. The result is that the peak to peak voltage of the square wave signal across the transmitter is double the voltage of the signal supplied to the motor driver. A DC voltage of 10V was supplied to the motor drivers and the square waves generated by the Arduino were connected to the input pins to produce square waves of 20 Vpp to power the transmitters.

Two square wave signals generated at two pins of the Arduino are shown in Figure 3.2. The first wave has no delay applied and the second has a delay of $3.55 \mu s$. The resulting signals measured across two transmitters when these square waves are amplified by the motor driver and supplied to the transmitters are shown in Fig 3.3. The Arduino code that was run to implement this delay sequence is included in the GitHub repository in Appendix A.

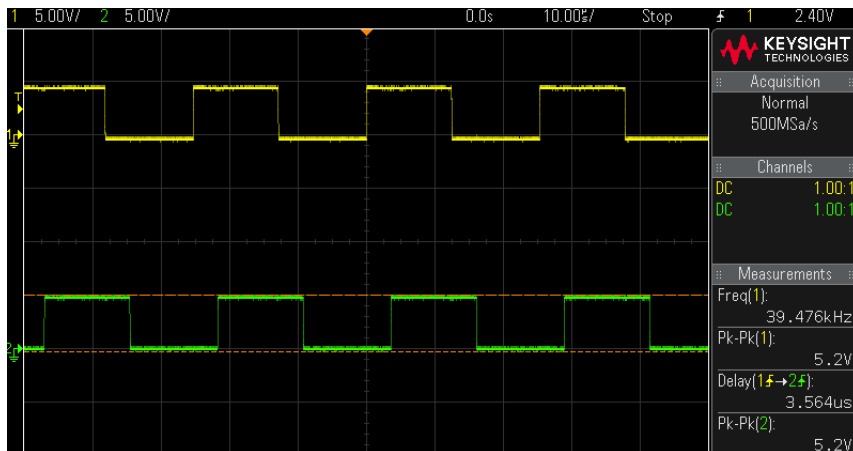


Figure 3.2: Two square wave signals generated at the pins of the Arduino. The first wave has no applied delay and the second has a delay of $3.55 \mu s$

When powered with the 20 V 40 kHz square waves the transducers emitted sinusoidal ultrasound waves. This was confirmed using the receivers which produce an electrical signal in response to acoustic waves. The voltage across a receiver placed in front of a single transducer is displayed in Figure ???. The frequency is 40 kHz, resembling the excitation signal. The peak voltage diminishes as the receiver is moved away indicating the inverse relationship between acoustic intensity and distance from the source. The value of the peak voltage when the receiver is placed as close as possible is 20 V.



Figure 3.3: Voltage signals measured across two transmitters when supplied with the signals in Figure 3.2 amplified to 20 Vpp by a L298N Dual H-Bridge Motor Driver.

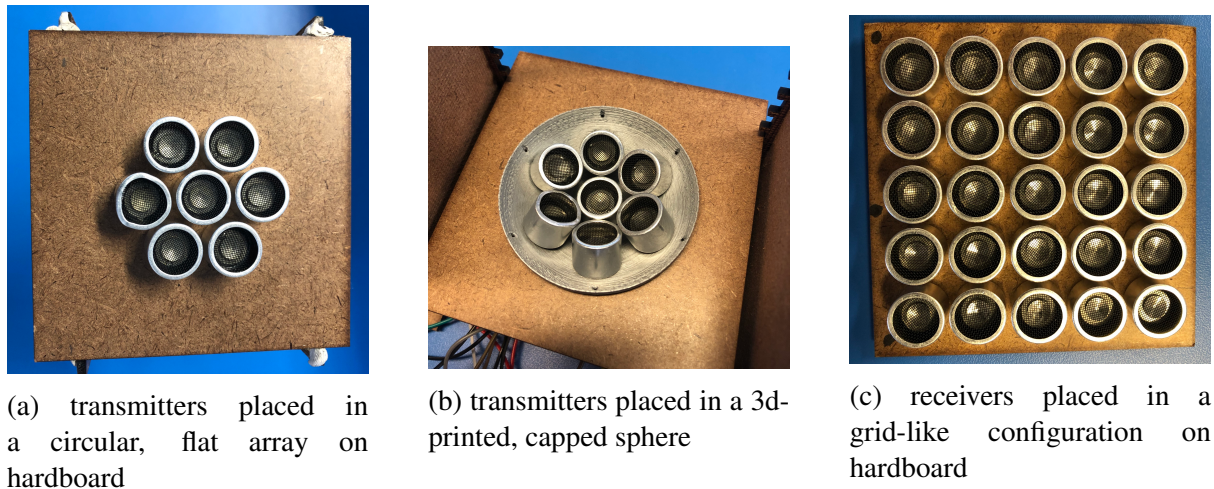


Figure 3.4: Configurations of transmitters and receivers for testing

3.3 Setup Design

After successfully powering the transducers with phased signals, a formal testing setup was designed.

Two different transmitter configurations were designed. The first configuration was a flat circular array of 6 transmitters plus a seventh central transmitter as shown in Figure 3.4a. The other configuration, shown in Figure 3.4b, placed the 7 transmitters inside a capped sphere, which physically places the transmitters at equal distances from a focal point.

In order to compare the resulting ultrasound fields generated by the transmitters when emitting at different phases, it was important to keep the positions that the voltage was measured at consistent throughout the different tests. It was decided that the best way to do this was to

3.3. SETUP DESIGN

have a square, grid-like array of receivers that could be placed at different, equally spaced heights. The voltage could then be measured at the same positions for each test and the results compared. The square array of receivers is shown in Figure 3.4c. Shafts were designed for each corner of the structure that have many slots for the receiver array to be placed in. The slots continue vertically up the shafts at 1 cm intervals so that the receiver array can be placed at different heights on the measuring stand.

Hardboard was used for the flat transmitter array, the receiver array, the shafts and additional supportive elements for the measuring stand structure such as struts. The hardboard was laser cut. The designs for the structure were done in SolidWorks. The capped sphere was designed in SolidWorks and 3d printed with plastic. PDFs for laser cutting the hardboard parts are included in Appendix C and the stl file of the capped sphere designed for 3d printing is included in the GitHub repository. The link to the repository is included in Appendix A.

The structure was assembled using superglue to fix the laser-cut parts together. The assembled structure is shown in Figure 4.2.

A co-ordinate system was defined in order to define the positions of each data reading so the results of different tests as well as the simulations could be compared. The coordinate system was also essential in defining the positions of the transmitters with respect to the positions of the data readings. The xy-coordinate system is displayed on the flat array of transmitters in Figure 3.5a with the x and y positions of the 7 transmitters defined. Figure 3.5b shows the full xyz-coordinate system that was used in measurements, plots of the results and simulations.

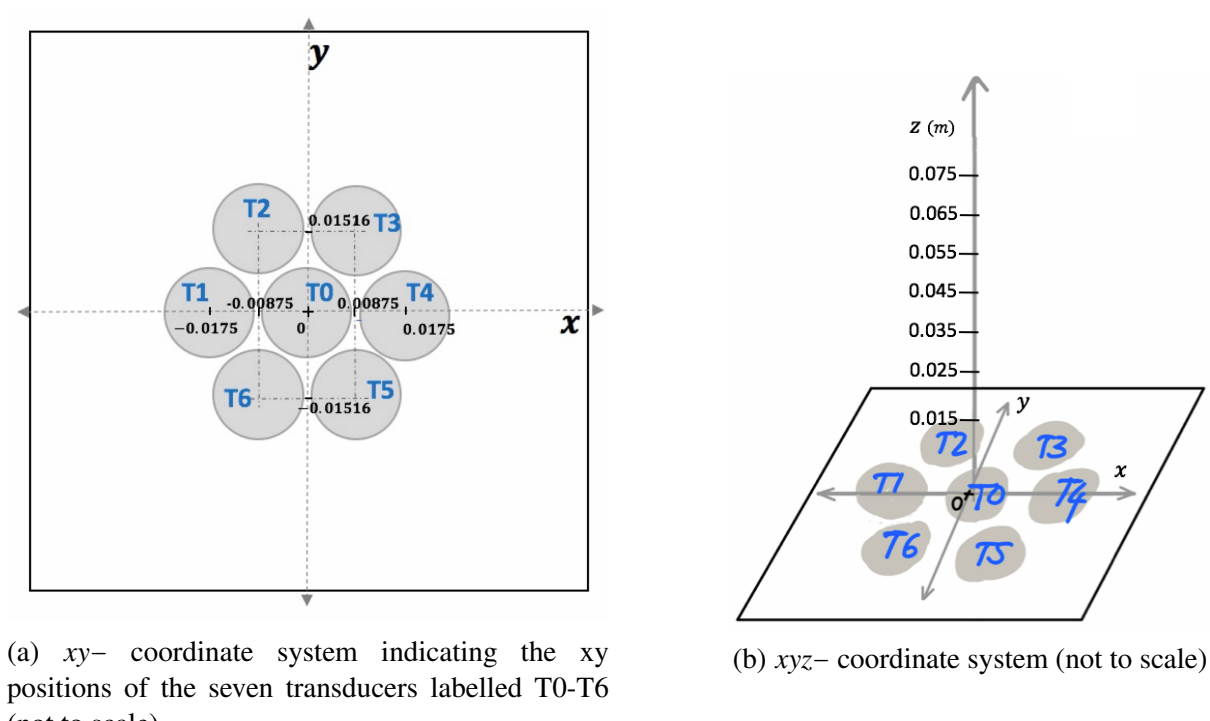


Figure 3.5: Coordinate systems used for measurements, plots of results and simulations

Chapter 4

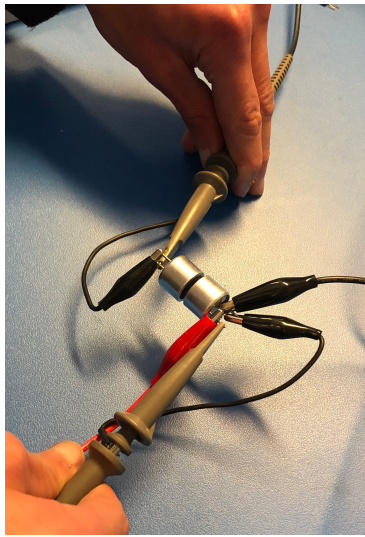
Implementation

4.1 Experimental Preparation

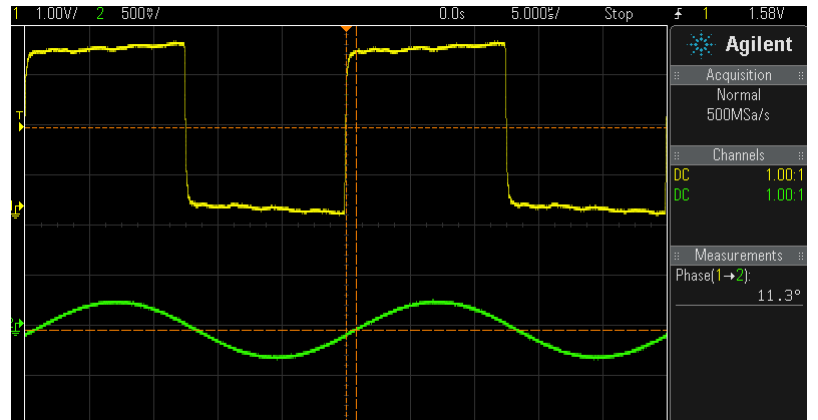
4.1.1 Polarity Test

The polarity of the transmitters had to be tested to ensure that the waves generated would all be of the correct phase. The transmitters and receivers do have a marking indicating the polarity; however, these markings are not reliable as reported by [16]. It is vital that the transmitters are all connected with the correct intended polarity for the desired wave interference to take place. If a transmitter's connections are swapped the wave emitted will be 180° out of phase to the intended wave and this will detract from the pressure in regions where it was intended to add to. It is not important for this project to test all the receivers' polarity as an oscilloscope is used to measure the peak to peak voltage across each receiver so if the wave is out of phase the peak to peak voltage measured will be the same as if it was in phase.

To test the transmitters' polarity a signal generator was set to generate a 40 kHz square wave, which was supplied to one of the transmitters. An oscilloscope probe was connected to the transmitter and a 40 kHz square wave was displayed on the oscilloscope screen as expected. Another oscilloscope probe was connected to another transmitter or receiver, which was placed face to face with the transmitter being powered. The two transmitters were placed as close to each other as possible and the phase difference between the two wave forms was compared. The second transmitter or receiver generated a 40 kHz sine wave. If the phase was close to 0° then the waves were considered in phase and the marked polarity correct. If the phase was close to 180° the waves were out of phase meaning the polarity was incorrect. This was repeated



(a) Transmitter Polarity Test: Two transmitters placed opposite each other with one being powered by a square wave. The signals generated at both transmitters displayed on the oscilloscope and the phase difference compared.



(b) Oscilloscope screenshot of the square wave supplied to one transmitter and the sine wave received by the other. The polarity of this transmitter (or receiver) is correct as the phase difference is small

Figure 4.1: Polarity Test

for all seven transmitters and they were all marked with the correct polarity.

4.2 Testing

The testing section is divided into the five individual tests that were implemented.

Test 1

For the first test the transmitters were placed in the flat circular array configuration and no delays were applied. The transmitters were put in place and connected to the driver boards. The Arduino was plugged into the computer and the code was uploaded.

A DC power supply was used to supply 10 V to the driver boards. The Arduino and driver board were connected to ground. A breadboard was used to make these connections. The full setup is shown in Figure 4.2.

The resulting acoustic field was measured by recording the peak-to-peak voltage of the sine

4.2. TESTING

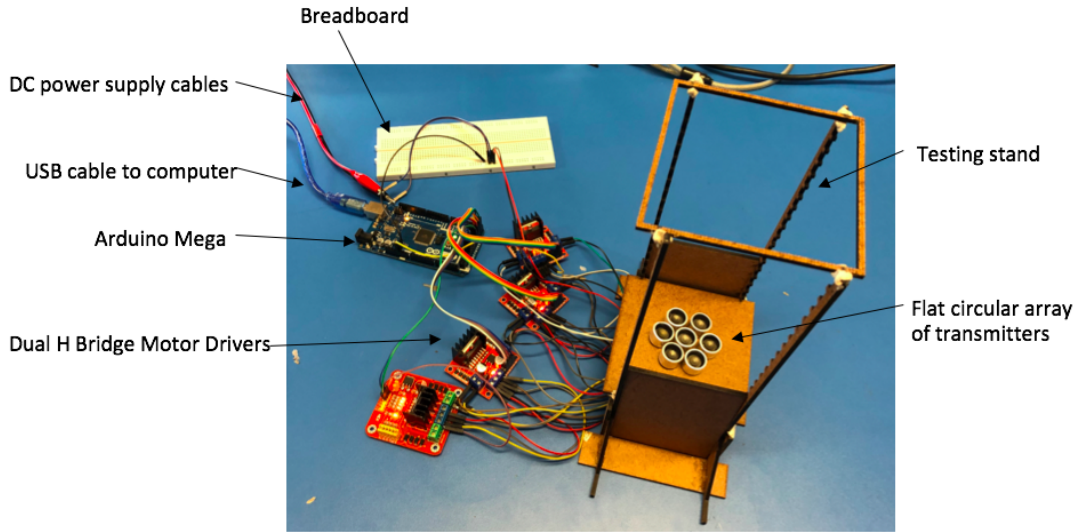


Figure 4.2: Experimental Setup

waves received at different points. The readings were taken using an oscilloscope (Agilent Technologies InfiniiVision Oscilloscope (DSO-X-2002A)). Starting with the receiver square array placed in the bottom slots of the shafts, the probe was connected to a receiver as shown in Figure 4.3 and the voltage observed was recorded in an excel spreadsheet, which is included in Appendix B. This was done for all the receivers in the array and then the array was moved to the next height and the process was repeated.

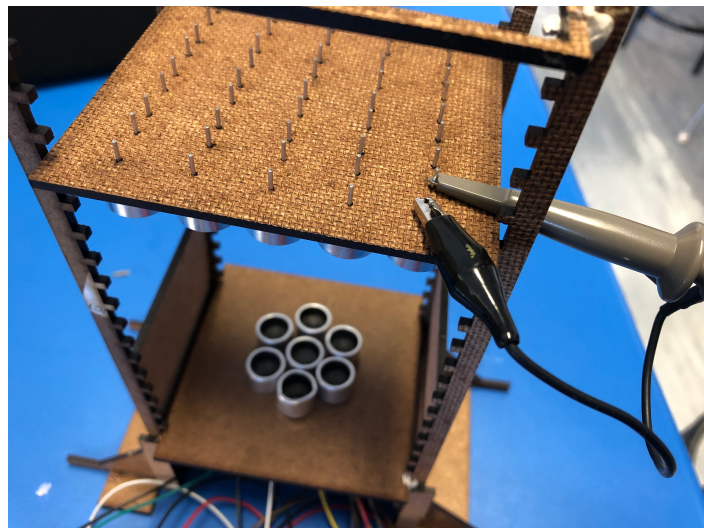


Figure 4.3: Oscilloscope probe measuring the voltage across a receiver

The signals sensed at the receivers were 40 kHz sine waves; however the amplitudes constantly changed as shown in the oscilloscope screenshot in Figure 4.4. To be able to read the peak voltage value the time segments were increased to 50 ms per division, so the envelope of the ultrasound signals indicating the peak voltage value could be observed. This is shown in Figure 4.6. Figure 4.5 is included to show the voltage signal at 2 ms per division as this shows how increasing the time scale helps the envelope of the wave to be observed.

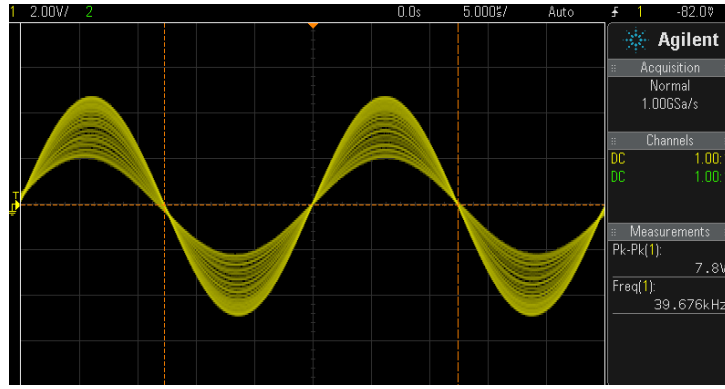


Figure 4.4: Signal generated across a receiver when placed opposite multiple emitting transmitters.



Figure 4.5: Signal generated across a receiver when placed opposite multiple emitting transmitters with timescale scaled up to 2 ms per division.

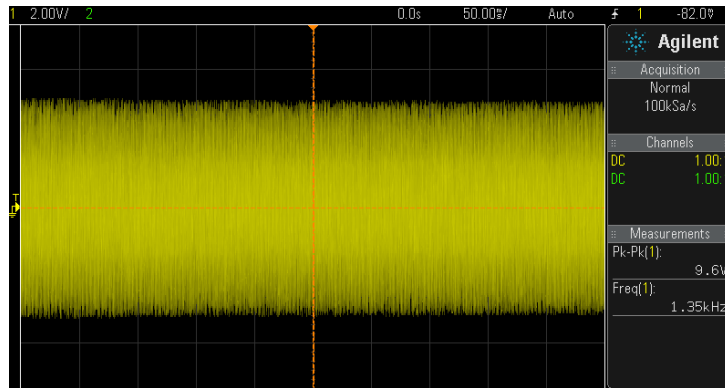


Figure 4.6: Signal generated across a receiver when placed opposite multiple emitting transmitters with timescale scaled up to 50 ms per division.

The following tests were implemented by applying delays to the different signals to create a high intensity region, or main lobe, around a particular focal point. The focal point was defined as $F = [x \ y \ z]$ where x, y and z represent the focal point's position on the axes defined in Figure 3.5. Before doing these tests it was necessary to calculate the delays necessary to focus the beam at each focal point. A MATLAB program was written to calculate the required delay values to be applied to each of the transducers' feeding signals to focus the main lobe

at the focal point. The transducers' positions and the position of the desired focal point are specified and the program calculates the delays that should be applied to the signals feeding each transducer. The MATLAB code is included in the GitHub repository in Appendix A.

Test 2

For the second test the array was phased to focus the resulting main lobe at $F = [0 \ 0 \ 0.05]$ m. The values of the delays required for this were calculated using the MATLAB program.

The program calculated that a delay of $8.7 \ \mu s$ should be applied to the central transducer's input signal and the other signals could be left at no delay. This makes sense as the signal emitted from the central transmitter is travelling a shorter distance than the signals from the other transmitters, and should therefore be emitted at a slight delay for the signals to meet at the focal point in sync. The Arduino code for this was written and is included in the GitHub repository. The code was uploaded to the Arduino, the power supply was turned on and the voltage readings were taken. The data recorded is included in Appendix B.

Test 3

After implementing the first two tests it was decided that taking many readings outside of the area around the focal point was not necessary as the results for these peripheral transducers were insignificant. Instead of reading the signals generated at all 25 receivers of the receiver array, the testing area was reduced to the central 9 receivers.

For the third test, a focal point was chosen as $F = [0.018 \ 0 \ 0.05]$ m. The delays were calculated using the MATLAB program. The delays were more varied than for the previous test. A timing diagram was drawn to be able to easily compare the signals' delays and ensure accuracy in coding. The delays returned by the MATLAB program for each transducer and the associated timing diagram are shown in Figure 4.7. The Arduino pins chosen to generate these signals for this test are also displayed. Each pin is described by the letter of the port it belongs to and the bit of that port that it is represented by. These pins were chosen for concise coding - signals that had the same delays were chosen to be in the same port.

The code to generate the signals with specified delays at the relevant pins of the Arduino was written and is included in the GitHub repository. The code was uploaded to the Arduino. To ensure the code was working correctly two oscilloscope probes were used to measure different signals generated at the relevant Arduino pins and the delays between them were checked for accuracy. For example Figure 4.8 shows the signals at A7 and C1 (or D29 and D36 as labelled on the Arduino Mega 2560). The delay measures $7.692 \ \mu s$ and the desired delay is $7.65 \ \mu s$ as

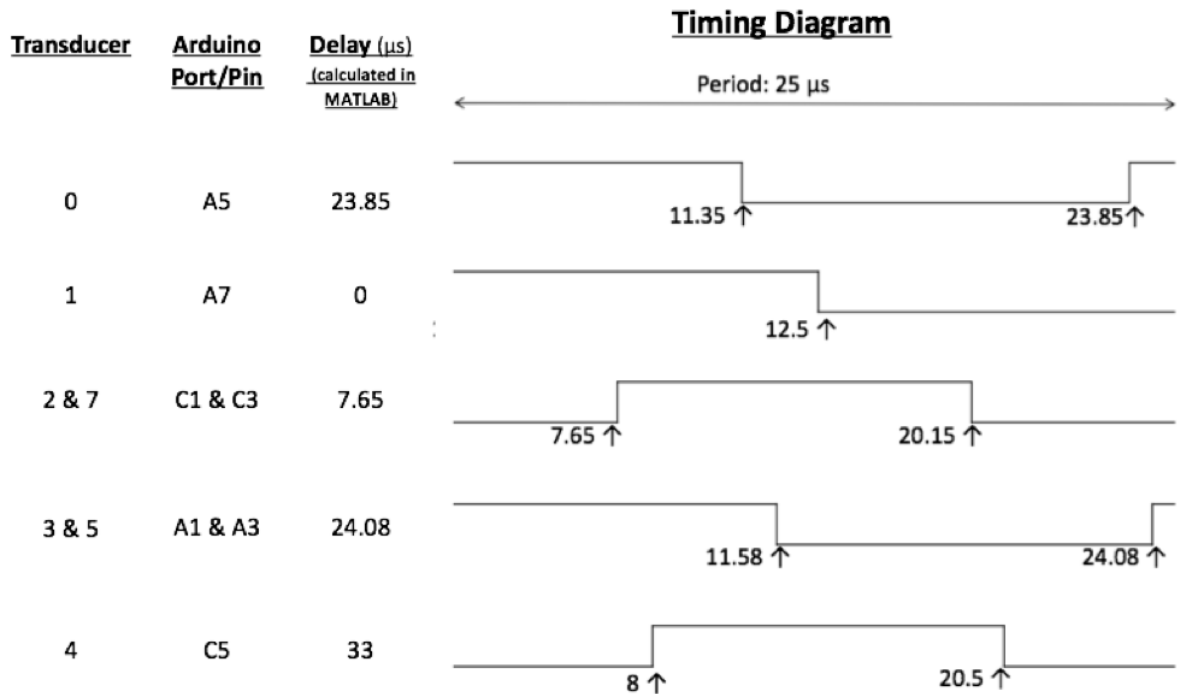


Figure 4.7: Timing diagram for the signals to be applied to the 7 transducers to focus at $F = [0.018 \ 0 \ 0.05] \text{ m}$

shown in Figure 4.7, which is within an acceptable tolerance. All the signals were checked. The power supply was then switched on and the voltage readings taken. The data recorded is included in Appendix B.

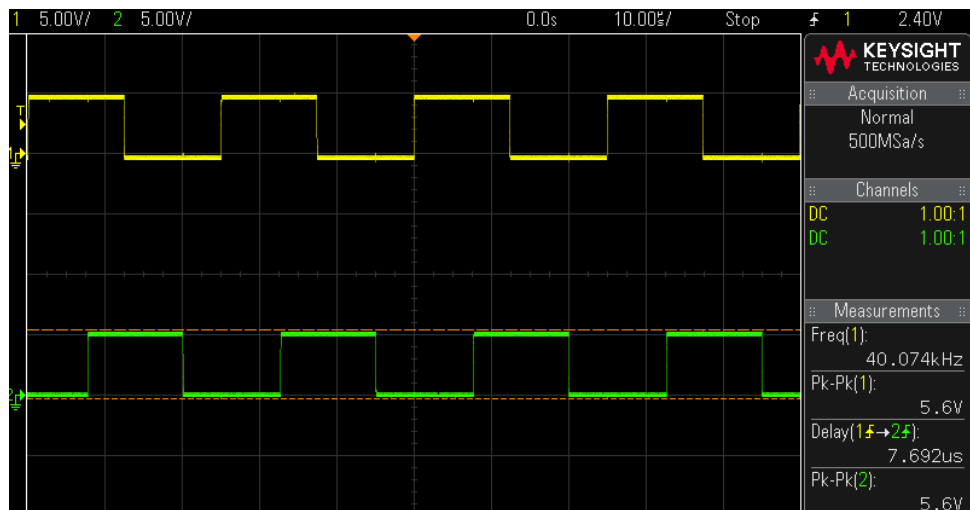


Figure 4.8: Signals generated at A7 and C1 (or D29 and D36 as labelled on the Arduino Mega 2560). The signal generated at A7 has no delay and the signal at C1 is at a delay of $7.65 \mu\text{s}$

Test 4

The next test was done for a focal point of $F = [0 \ 0.018 \ 0.05] \text{ m}$. Repeating the process from the previous test, the delays were calculated and a timing diagram was drawn as shown

in Figure 4.9. This diagram was used to write the Arduino code as included in the GitHub repository. The code was uploaded and the signals generated at the Arduino pins were checked for accuracy using the oscilloscope.

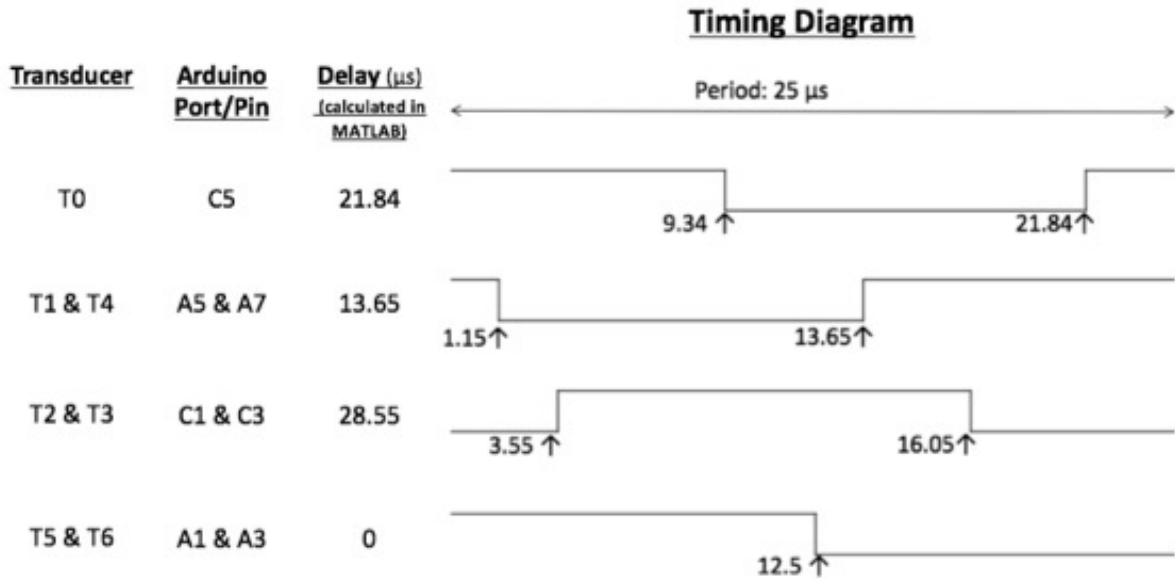


Figure 4.9: Timing diagram for the signals to be applied to the 7 transducers to focus at $F = [0 \ 0.018 \ 0.05] \text{ m}$

After ensuring the signals were at accurate timing delays, the DC power supply was set to 10 V and supplied to the motor drivers through the breadboard connections. The voltage readings were taken and are included in Appendix B.

Test 5

The final test was to be done using the capped sphere array. The transmitters were transferred to the capped sphere and connected to the driver boards. The Arduino code for no delays was uploaded to the Arduino and the signals generated at the pins were verified using the oscilloscope. The receiving array was placed at the lowest level of the measuring stand and the voltage readings were taken. Further readings were taken with the receiving array at higher slots on the shafts of the measuring stand. The recorded data is included in Appendix B.

4.3 Simulations

A MATLAB program, included in Appendix A, was created to simulate the ultrasound fields generated by the transmitters when different phases are applied. This was done by calculating the values of the pressure waves emitted from the seven transmitters at a point and summing

4.3. SIMULATIONS

them to obtain the total pressure value for that point. Formula 2.4 was used to calculate the value of the pressure wave due to each source. This was done for many co-ordinates in the x-y-z space, which were plotted as coloured points with the colour representing the pressure value at that point.

The pressure attenuation due to beam divergence, as included in Formula 2.4, was considered for this simulation. The attenuation due to absorption was not considered as the absorption for ultrasonic waves in the lower frequency range (20 kHz - 100 kHz) when propagating through air over small distances is negligible. The attenuation of 50 kHz ultrasound in air at 20°C and 60% humidity is about 1 dB/m.[20] This corresponds to less than a percent attenuation over the 8 cm distance considered for this experiment. This small attenuation factor would not affect the simulations and was therefore excluded.

Several simulations were generated from this program to observe the various pressure fields being generated by the different transmitter configurations with the different delay sequences applied. The simulations were used to validate the experimental results. Several plots are included in the Results section, which follows.

Chapter 5

Results

This chapter presents the experimental results and simulations for each test. The data recorded in the experimental tests was processed into plots that could be analysed and compared. Both the plots of the experimental data and the simulations were generated in MATLAB.

The data is difficult to represent in an easily understood format. This is because it is four dimensional data as each recording has an x, y and z position as well as a voltage value. The data was therefore plotted with colour representing the voltage value. Each dot on the plot represents a data point plotted according to its position. The points along the x-axis have been more spaced out to prevent overlapping. The colour scale representing voltage values is included for each plot.

In order to compare the experimental results to an accurate model, the acoustic field for each test was simulated using the MATLAB program created, which is included in the GitHub repository in Appendix A. The simulation for each test is included after the plot of the experimental results for each test so direct comparisons can easily be made.

Test 1

Figure 5.1 shows the experimental results for the flat circular array of transmitters when no delays were implemented and Figure 5.2 shows the corresponding simulation. Higher voltage readings were recorded in the central region of the x,y plane and close to 0 along the z-axis as this is the region closest to the transmitters. The experimental results resemble the simulation in Figure 5.2.

Test 2

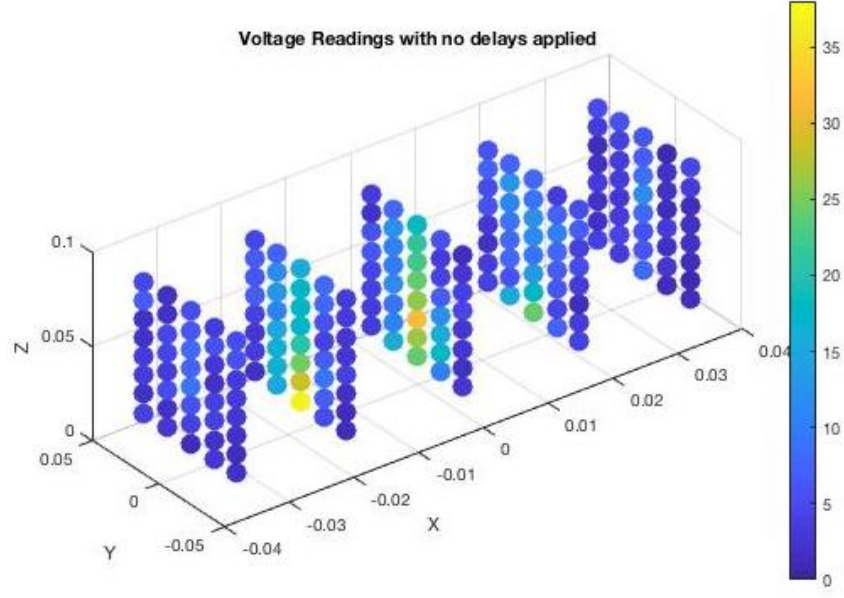


Figure 5.1: Plot of the voltage readings of the acoustic field produced by the circular array of transmitters when no delays are implemented.

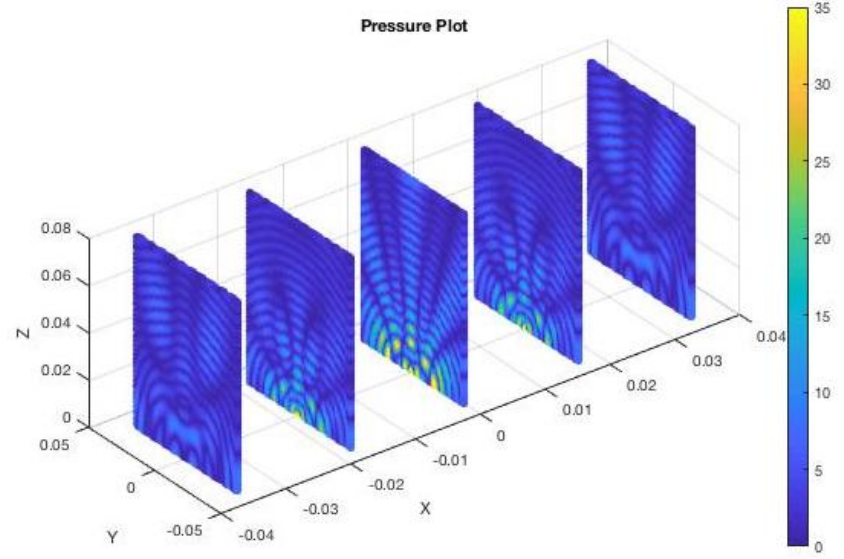


Figure 5.2: Simulation of the acoustic pressure field produced by the circular array of transmitters when emitting in phase

Figure 5.3 shows the experimental results for the flat circular array of transmitters when a delay sequence was implemented for a focal point of $F = [0 \ 0 \ 0.05]m$ and Figure 5.4 shows the corresponding simulation. These plots show resemblance in that there is a significant central beam of higher pressure.

The plots of the experimental results for the following tests have less data points than the previous ones. The reasoning for this is explained in the Implementation Section. However, this might lead to confusion in interpreting the plots. The simulations continue to have five

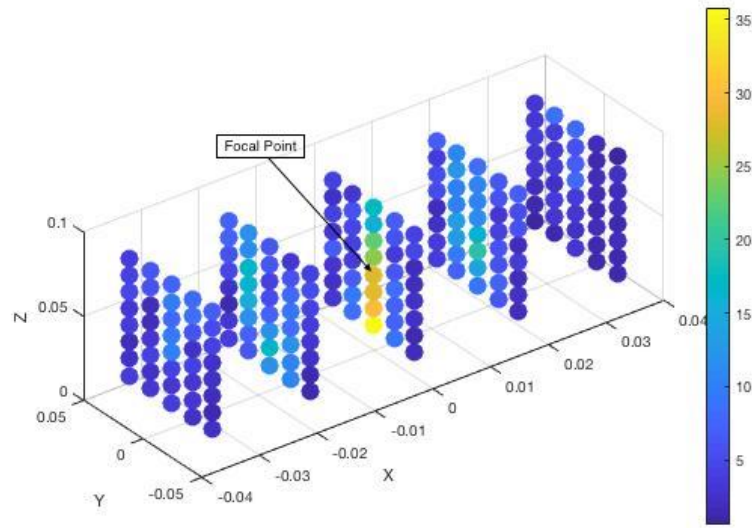


Figure 5.3: Plot of the voltage readings of the acoustic field produced by the circular array of transmitters when a delay is applied to focus the beam at $F = [0 \ 0 \ 0.05] \text{ m}$

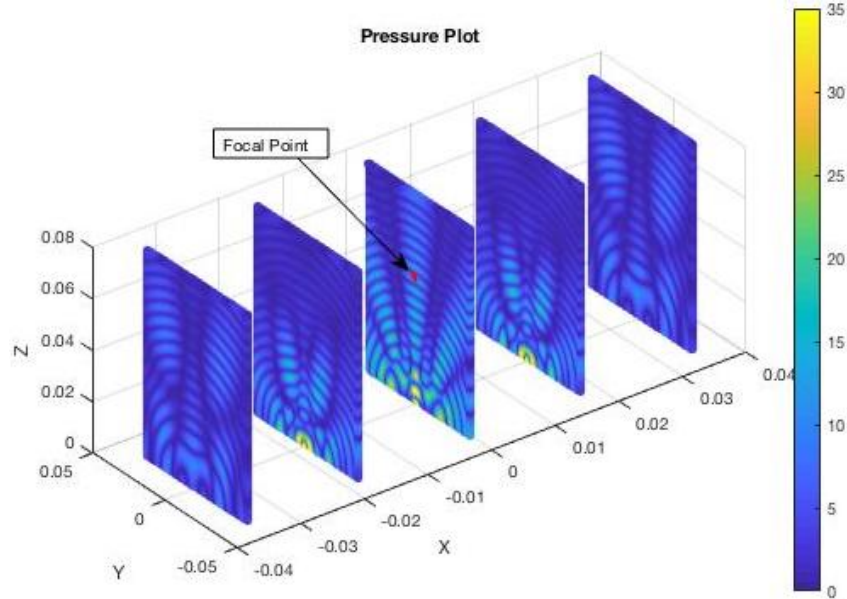


Figure 5.4: Simulation of the acoustic pressure field produced by the circular array of transmitters when a delay is applied to focus the beam at $F = [0 \ 0 \ 0.05] \text{ m}$

'slices' along the x-axis whereas, the plots of the experimental results only have three. The inner three slices of the simulation plots correspond to the experimental results for these three tests. These 'slices' are at the x values of the data recorded: $x = [-0.085, 0, 0.085]$. These three inner slices of the simulations still display a slightly larger region than that of the experimental results plots as they extend slightly further along the y- and z-axes. The simulations were kept over the larger region in order to display more of the pressure field so the effects of the phased array system can be observed in more detail.

Test 3

Figure 5.5 shows the experimental results for the flat circular array of transmitters when a delay sequence was implemented for a focal point of $F = [0.018 \ 0 \ 0.05] \text{m}$ and Figure 5.6 shows the corresponding simulation. The region of high intensity around the focal point shows up clearly in both plots.

There are two significantly high voltage readings on the opposite side of the x-axis to the focal region in Figure 5.5. At first this seems to be inconsistent with the expected results. However, on close analysis of Figure 5.6, it can be observed that there is a region of high pressure here due to a transmitter being located directly below it. The voltage readings recorded at $(-0.018, 0, 0.045)$ and $(0.018, 0, 0.045)$ are 16.1 V and 21.3 V respectively. This shows that at the desired focal region height of 0.05 m the pressure is highest at 0.018 m along the x-axis as desired.

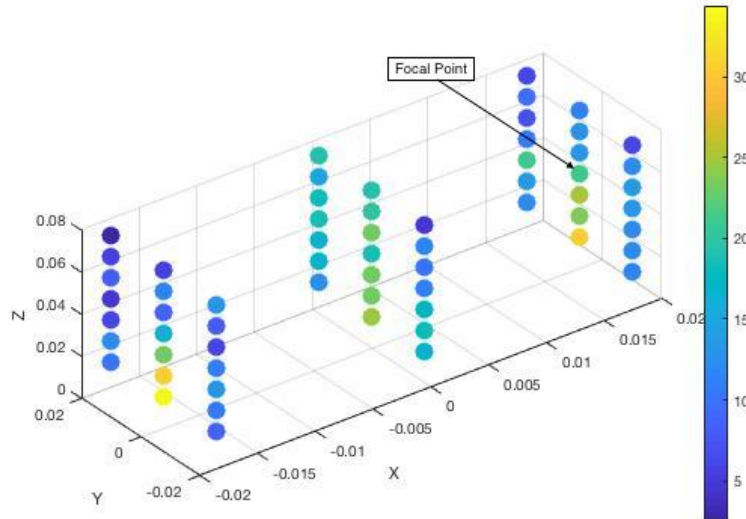


Figure 5.5: Plot of the voltage readings of the acoustic field produced by the circular array of transmitters when a delay is applied to focus the beam at $F = [0.018 \ 0 \ 0.05] \text{ m}$

Test 4

Figure 5.7 shows the experimental results for the flat circular array of transmitters when a delay sequence was implemented for a focal point of $F = [0 \ 0.018 \ 0.05] \text{m}$ and Figure 5.8 shows the corresponding simulation. The voltage readings for this test decreased significantly compared to previous tests. The maximum voltage recorded was 18.5 V whereas the maximum voltage for Test 1, 2 and 3 were 24.1 V, 35.8 V, and 34.4 V respectively. Due to this, the colour-scale for the plot of the experimental results, Figure 5.7, was adjusted; therefore the colours in this

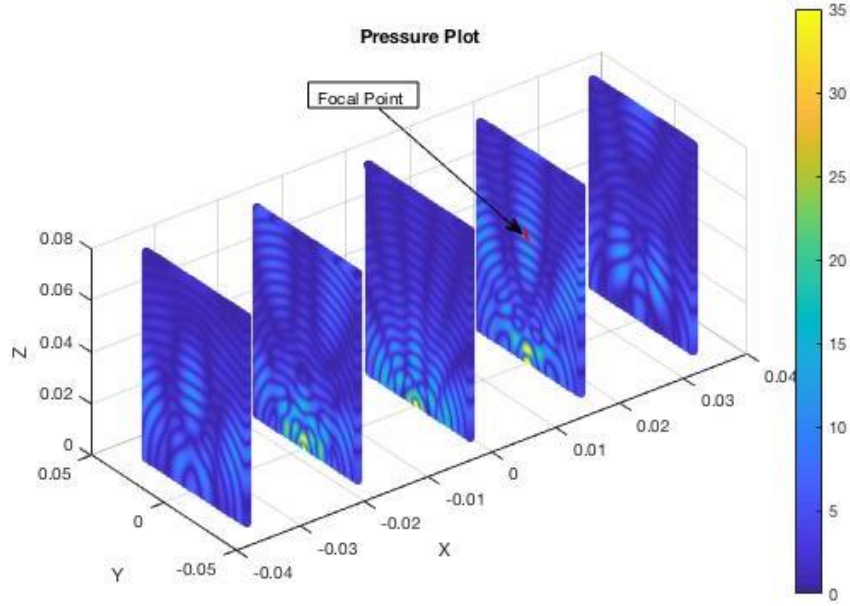


Figure 5.6: Simulation of the acoustic pressure field produced by the circular array of transmitters when a delay is applied to focus the beam at $F = [0.018 \ 0 \ 0.05] \text{ m}$

plot cannot be directly compared to the previous plots.

Figure 5.7 clearly shows that there are higher voltage readings in the focal region. The delay sequence has successfully created a region of higher pressure in the desired region. However, the overall decrease in voltage values is a concern. The simulation in Figure 5.8 does not indicate that the pressure values, which correspond to the voltage, are less than for previous tests.

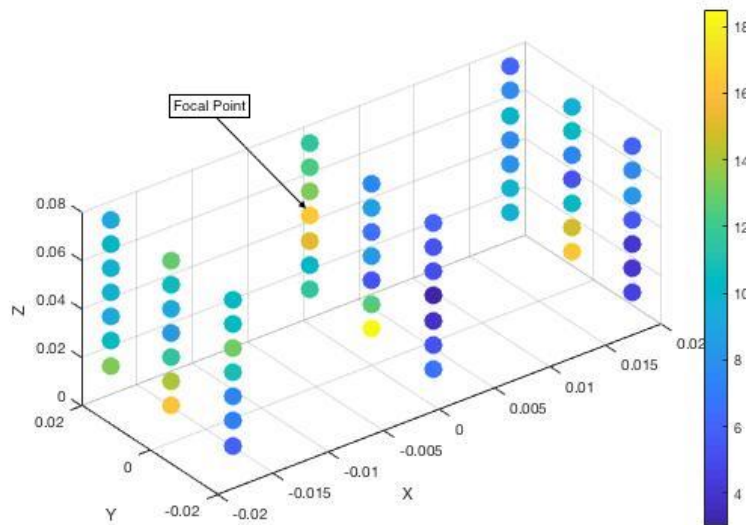


Figure 5.7: Plot of the voltage readings of the acoustic field produced by the circular array of transmitters when a delay is applied to focus the beam at $F = [0 \ 0.018 \ 0.05] \text{ m}$

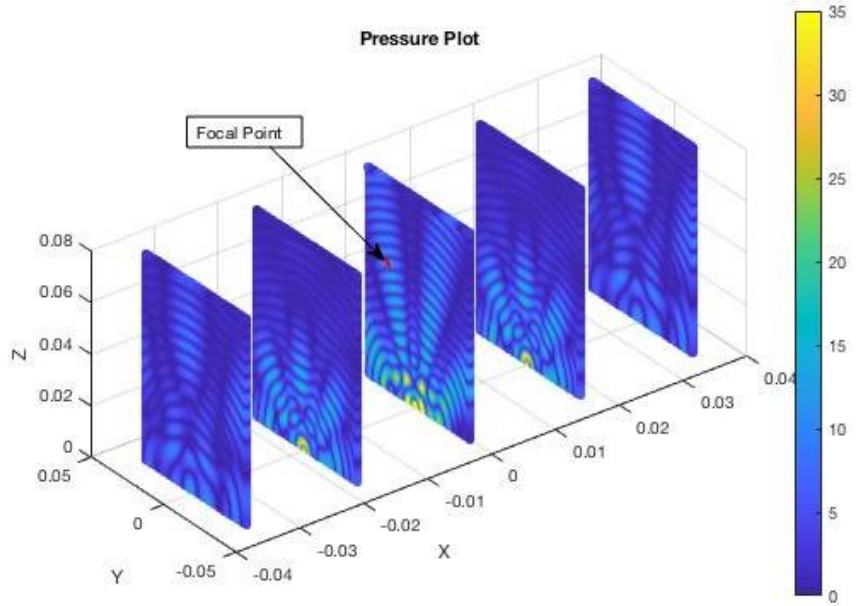


Figure 5.8: Simulation of the acoustic pressure field produced by the circular array of transmitters when a delay is applied to focus the beam at $F = [0.018 \ 0 \ 0.05]$ m

Test 5

Figure 5.9 shows the experimental results for the capped sphere array of transmitters and Figure 5.10 shows the corresponding simulation.

The capped sphere configuration places the transmitters slightly below the x-y plane in the testing stand. This means that the transmitters are at negative positions on the z-axis. Therefore the point (0,0,0) in Figure 5.9 should be compared to the point (0,0,0.02) in the previous plots of the experimental results to ensure that the data points are at the same distances above the central transmitter. Since the capped sphere was designed to focus the intensity at 0.05 m above the central transmitter, this corresponds to a focal point of $F = [0 \ 0 \ 0.03]$ in the xyz space.

The voltage readings for this test were also lower than for Tests 1-3. The maximum voltage was 22.05, which was at the position (0,0,0). The colour scale has been adjusted for these lower voltage values.

Additional simulations were implemented to visualize the beam patterns generated by the different tests in a three dimensional space. These are shown in Figure A.1 in Appendix A. These simulations show more clearly the different regions of constructive interference or the different lobes of the acoustic fields generated.

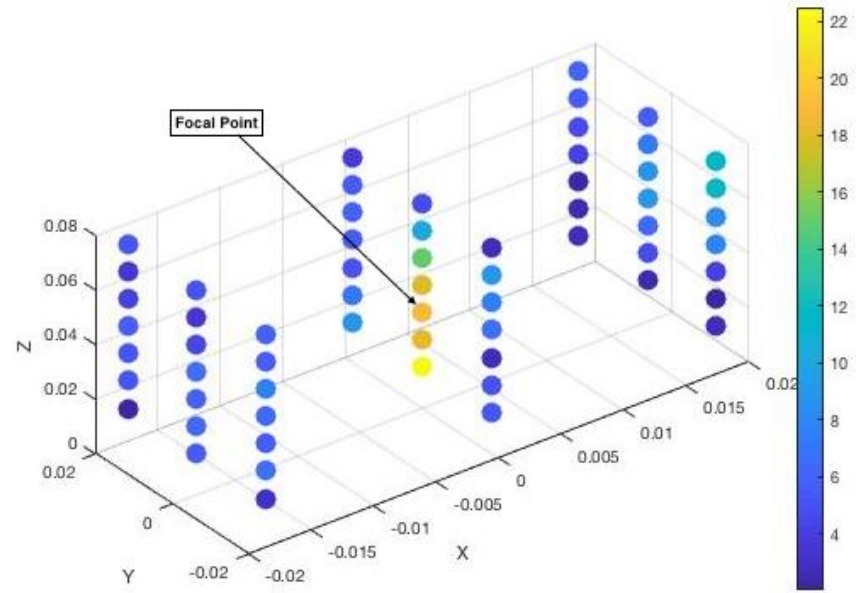


Figure 5.9: Plot of the voltage readings of the acoustic field produced by the capped sphere of transmitters

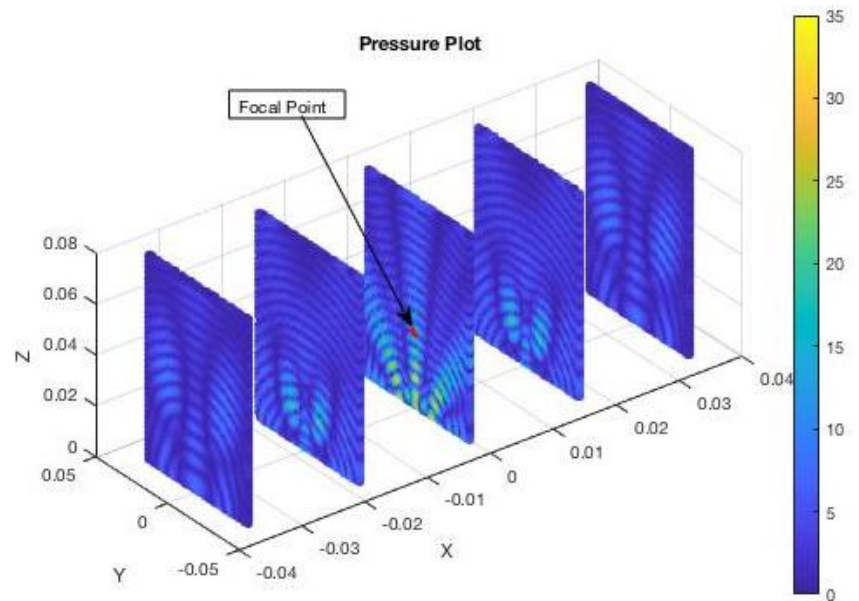


Figure 5.10: Simulation of the acoustic pressure field produced by the capped sphere of transmitters

Chapter 6

Discussion

This chapter discusses the findings deduced from the results. Both the successes and the shortcomings of the tests are described.

The simulations visually resemble the experimental results in all the tests, which shows that the system developed can successfully generate regions of high pressure at desired locations.

The effectiveness of the phased array system in maximising the pressure amplitude can clearly be observed in the results. By comparing Figure 5.1, the results of Test 1, when no delays were applied to the system, and Figure 5.3, the results of Test 2, when a delay was implemented to focus the main lobe at $F = [0\ 0\ 0.05]m$ the significant increase in the voltage values along the central line of the z axis when a delay sequence is implemented can be observed. This is indicated by the increase in yellow dots. For example the voltage value at the position $(x,y,z)=(0,0,0,045)$, is 21,9 V for Test 1 and 27,7 V for Test 2. Since the voltage values correspond to the pressure, it is clear that there is an increase in pressure in the desired focal region when the delay sequence is implemented.

It can also be observed that the energy is more dispersed when no delays are applied, as shown by the high voltage values at (-0.0175, 0, 1.5) and (-0.0175, 0, 2.5) in Figure 5.1. The high voltage values in Figure 5.3 are concentrated in the central region. This shows the effectiveness of a phased array system to not only produce a desired region of high intensity but also to eliminate undesired regions of intensity.

The decrease in the voltage values for Test 4 and Test 5 was at first confusing. However, on closer analysis of the test design, these results can be understood. The lower voltages recorded in Test 4 are most likely as a result of the transmitters' positions. The focal point in Test 4 is

$F = [0 \ 0.018 \ 0.05]$. The approximate position of this on the x-y plane is indicated by arrow 1 in Figure 6.1. This is positioned in the space between two transmitters and therefore, does not have a transmitter located directly below it, which is the case for the other tests. For example, Test 3 had a focal point of $F = [0.018 \ 0 \ 0.05]$. Its approximate position on the x-y plane is indicated by arrow 2 in Figure 6.1. There is a transmitter directly below this focal point and therefore the acoustic energy reaching the point is much higher.



Figure 6.1: The flat, circular array of transmitters with arrow 1 and arrow 2 indicating the approximate positions of the focal points on the x-y plane for Test 4 and Test 3 respectively

This observation shows that the acoustic energy is significantly higher directly above the vibrating piezoelectric crystal than at an angle. The simulation program was based on Equation 2.4, which describes the pressure of an acoustic wave at a distance from a point source, which emits an omnidirectional wave.[2] This means that the pressure amplitude calculated by the simulation at equal distances from a point source is equal regardless of the direction.

The unexpectedly low voltage values measured for Test 4 could be due to the fact that the transmitters are not ideal point sources and therefore do not emit equal amplitudes of ultrasound in all directions. This would explain why the delay sequence implemented to create a region of high pressure at a focal point of $F = [0 \ 0.018 \ 0.05]$ succeeds in maximising the pressure in this region compared to the other regions in the plot but does not generate an acoustic field that reaches voltages that are as high as the other tests and does not completely resemble the simulation in Figure 5.8.

The relatively low voltage values for Test 5 were also unexpected. The capped sphere array of transmitters has been reported as the most effective configuration for producing a region of high intensity.[21] Analysing the simulation in Figure 5.10 reveals that the pressure values predicted for this test are actually less than those for previous tests. The highest pressure values observed in Figure 5.10 are at approximately 25 whereas the simulations for previous tests had spots of up to 35. This is, however, due to the fact that the transmitters in the configuration for the simulation in Figure 5.10 are slightly below the z axis. If the focal points in Figure 5.10 and Figure 5.4 are compared, it can be observed that the pressure in the focal point of Figure 5.10 appears to be slightly more than that of Figure 5.4 as indicated by the slightly greener colour.

Overall, the experimental results, as well as the simulations, tend to show the highest voltage value directly above a transmitter. This implies that proximity to a transmitter is a dominant factor in determining the acoustic pressure at a point. It also indicates that the transmitters are not ideal omnidirectional point sources. The transmitters appear to emit a pressure wave of higher amplitude perpendicular to the transmitter surface than at an angle. This finding highlights a need to further research transducer designs and the effects the design has on the properties of the ultrasound emitted.

Since these tests implemented a phased array system of airborne ultrasound, the results cannot be directly interpreted in relation to ultrasonic botanical extraction, which involves ultrasound transmitted in a liquid medium. The acoustic attenuation of an acoustic wave propagating through a liquid medium is significantly less than an acoustic wave of the same frequency propagating through air. Therefore, an ultrasonic phased array system implemented in a liquid medium is likely to be more effective at generating regions of high pressure than the system implemented in this project.

Chapter 7

Conclusions

The tests have clearly shown that a phased array system can create a main lobe around a focal point with much higher voltage readings than an array where no signal delays are implemented. This outcome is also indicated in the simulations.

What is interesting though is the failure of Test 3 compared to the result expected from the simulation that was run. This demonstrates the need in practice to ensure actual equipment used is optimised for idiosyncrasies and the actual operating environment. In this particular instance the practical optimal focal point to maximise pressure in the main lobe may differ from simulated results due to the transducers being used not being perfectly omnidirectional in their propagation of ultrasound waves. Further testing would be required to determine this point.

In considering ultrasound assisted extraction it would seem that implementing a phased array could add value. A phased array system would allow a region of high intensity within the plant slurry to be generated, which would cause cavitation to occur and plant compounds to be released. The main lobe could then be steered to different locations in the plant slurry, allowing cavitation activity to occur in all regions. This process could be effective in achieving a more complete extraction as it ensures that cavitation activity occurs throughout the plant slurry.

In order to assess the potential of a phased array system for ultrasound botanical extraction it is, however, necessary to carry out tests in a liquid medium as the properties of ultrasound in liquids is very different than in air.

Chapter 8

Recommendations

Tests in a Liquid Medium

In order to assess whether a phased array system would be effective in Ultrasound-assisted extraction, tests have to be implemented in a liquid medium. The properties of ultrasound in a liquid medium are significantly different than in air. Therefore, the results of similar tests to those done in this project implemented in a liquid medium might produce very different results. These results would give more valuable insight into the potential of a phased array ultrasonic system for botanical extraction.

If the tests are implemented in a liquid medium, a simple, affordable method to test for regions of high intensity is the aluminium foil test.[22] Other methods

Transducer Designs Further research should be done into the design of suitable transducers for an effective system to be implemented. Affordable, immersible transducers that consume less power need to be designed.

Future designs of ultrasound botanical extractors could look into omnidirectional transducer designs, which have recently emerged as having potential in underwater sensor applications.[23] The spherical design could be effective in generating a more uniform cavitation field of higher intensity as the ultrasound would be transmitted in all directions.

Bibliography

- [1] Olympus, “Ultrasonic transducers technical notes,” 2006.
- [2] T. Szasz, “Advanced beamforming techniques in ultrasound imaging and the associated inverse problems,” 10 2016.
- [3] Arduino mega 2560 r3. [Online]. Available: <http://electrobist.com/wp-content/uploads/2018/06/mega-1-1.jpg>
- [4] How to use the l298n dual h-bridge motor driver. [Online]. Available: <https://www.bananarobotics.com/shop/How-to-use-the-L298N-Dual-H-Bridge-Motor-Driver>
- [5] D. Panda and S. Manickam, “Cavitation technology—the future of greener extraction method: A review on the extraction of natural products and process intensification mechanism and perspectives,” *Applied Sciences*, vol. 9, 02 2019.
- [6] P. R. Gogate and A. Pandit, “Design and scale-up of sonochemical reactors for food processing and other applications,” 2015.
- [7] P. Gogate and P. Patil, *Sonochemical Reactors*, 08 2017, pp. 255–281.
- [8] P. R. Gogate and A. B. Pandit, “Hydrodynamic cavitation reactors,” Institute of Chemical Technology, Mumbai, India, Tech. Rep., 2017. [Online]. Available: https://traxxys.com/wp-content/uploads/2017/05/3.2.2_Technology_Report_Hydrodynamic_Cavitation_Gogate_Pandit.pdf
- [9] M. C. Ziskin, “Fundamental physics of ultrasound and its propagation in tissue.” *Radiographics : a review publication of the Radiological Society of North America, Inc*, vol. 13 3, pp. 705–9, 1993.
- [10] K. A. Roy, “Demonstrations in ultrasound imaging and beam steering using phased arrays,” 2015.
- [11] N. M. Tole and H. Ostensen, *Basic physics of ultrasonographic imaging*. World Health Organization, 2005.

BIBLIOGRAPHY

- [12] R. E. Berg, “Sound,” Aug 2019. [Online]. Available: <https://www.britannica.com/science/sound-physics>
- [13] R. B. Mitson and K. A. Johannesson, *Fisheries Acoustics - a Practical Manual For Aquatic Biomass Estimation*. Food at Agriculture Organization of the United Nations, 1983. [Online]. Available: <http://www.fao.org/3/X5818E/x5818e05.htm>
- [14] J. Poguet, A. Garcia, J. Vazquez, J. Marguet, and F. Pichonnat, “Phased array technology concepts, probes and applications,” <http://www.imasonic.com/Papers/PA2-02.pdf>, June 2002.
- [15] V. F.-G. Tseng, S. Bedair, and N. Lazarus, “Phased array focusing for acoustic wireless power transfer,” *IEEE Transactions on Ultrasonics, Ferroelectrics, and Frequency Control*, vol. PP, pp. 1–1, 11 2017.
- [16] A. Marzo, T. Corkett, and B. Drinkwater, “Ultraino: An open phased-array system for narrowband airborne ultrasound transmission,” *IEEE Transactions on Ultrasonics, Ferroelectrics, and Frequency Control*, vol. PP, pp. 1–1, 11 2017.
- [17] T. Carter, S. Seah, B. Long, B. Drinkwater, and S. Subramanian, “Ultrahaptics: Multi-point mid-air haptic feedback for touch surfaces,” 10 2013, pp. 505–514.
- [18] T. Allen, “Re: Parts for diy ultrasonic sensor, difference im ultrasonic transducers and recivers? [blog comment],” October 29 2012. [Online]. Available: <http://forums.parallax.com/discussion/143420/part-for-diy-ultrasonic-sensor-difference-im-ultrasonic-transducers-and-recivers>
- [19] Admin, “How to control arduino pins from registers without digitalWrite and digitalread,” Jan 2018. [Online]. Available: <https://www.epromszone.com/how-to-control-arduino-pins-from-registers-without-digitalwrite-and-digitalread/>
- [20] A. Vladišauskas and L. Jakevičius, “Absorption of ultrasonic waves in air,” *Ultragarsas (Ultrasound)*, vol. 50, no. 1, 2004.
- [21] A. Marzo, A. Barnes, and B. Drinkwater, “Tinylev: A multi-emitter single-axis acoustic levitator,” *Review of Scientific Instruments*, vol. 88, p. 085105, 08 2017.
- [22] B. Verhaagen and D. F. Rivas, “Measuring cavitation and its cleaning effect,” *Ultrasonics Sonochemistry*, vol. 29, p. 619–628, 2016.
- [23] S. Sadeghpour, S. Meyers, J.-P. Kruth, J. Vleugels, M. Kraft, and R. Puers, “Resonating shell: A spherical-omnidirectional ultrasound transducer for underwater sensor networks,” *Sensors*, vol. 19, no. 4, p. 757, 2019.

Appendix A

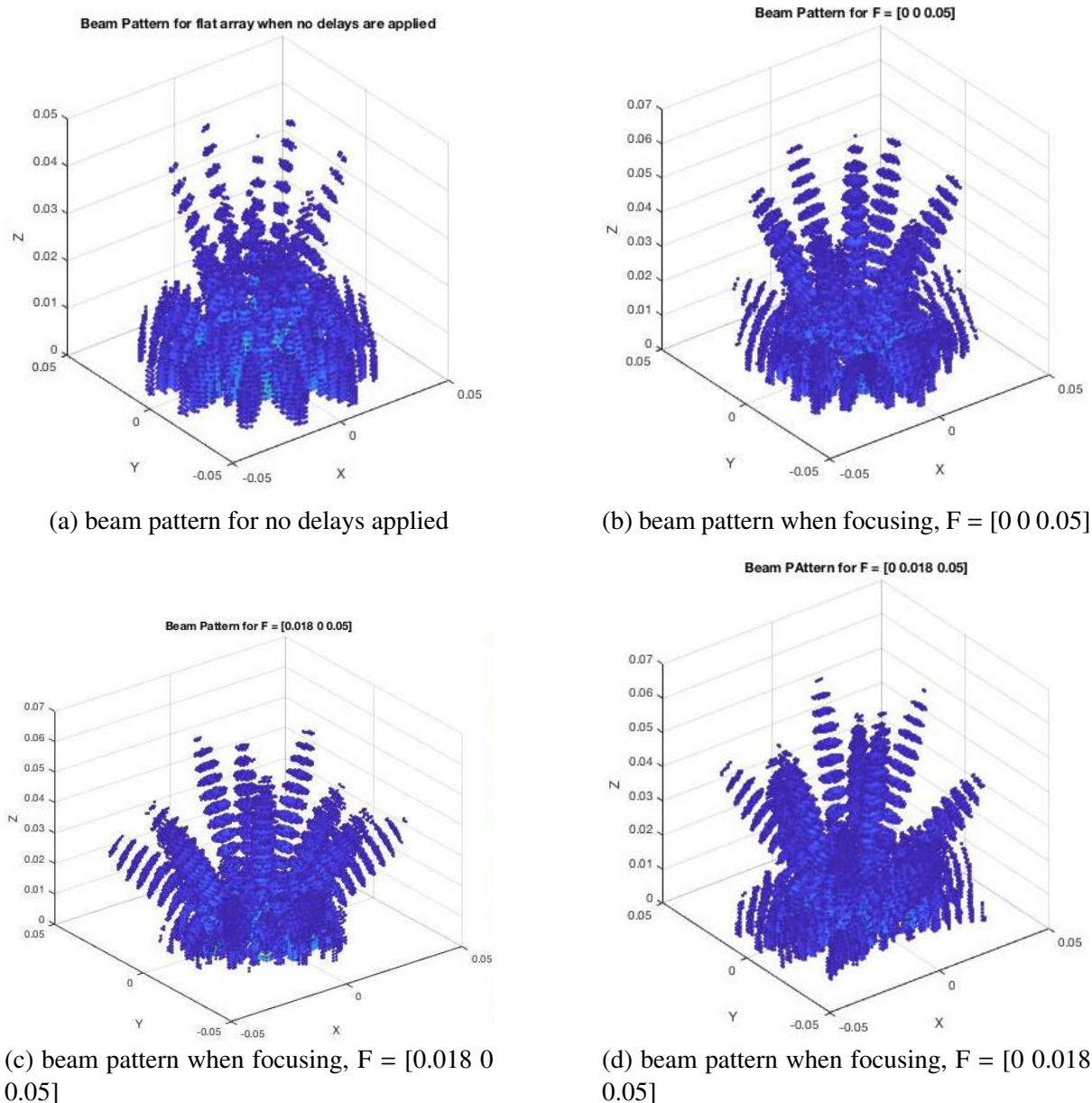
A.1 MATLAB and Arduino Code

The MATLAB and Arduino code written for this project can be found in the Github repository:
<https://github.com/marionboynton/Ultrasound-Phased-Array-project.git>

A.2 MATLAB simulations of beam patterns for Tests 1 - 4

A.2. MATLAB SIMULATIONS OF BEAM PATTERNS FOR TESTS 1 - 4

Figure A.1: Beam Patterns Simulated for Different Tests



Appendix B

B.1 Tables of Experimental Results

Table B.1: Results for the tests done with the linear flat array with no delays implemented (no delays) and focusing at $F = [0 \ 0 \ 0,05]$ (z focus)

Position			Voltage (Vpp)	
x	y	z	no delays	z focus
-0,035	-0,035	0,015	2,2	2,4
-0,035	-0,018	0,015	2,4	2,6
-0,035	0	0,015	1,6	3,6
-0,035	0,018	0,015	2,6	2,8
-0,035	0,035	0,015	4	3,4
-0,018	-0,035	0,015	1,6	1,6
-0,018	-0,018	0,015	7	10,7
-0,018	0	0,015	7,4	11,9
-0,018	0,018	0,015	12,9	6,4
-0,018	0,035	0,015	2,2	3,8
0	-0,035	0,015	2,6	1,8
0	-0,018	0,015	9	9,2
0	0	0,015	24,1	35,8
0	0,018	0,015	16,7	8,4
0	0,035	0,015	3	3
0,018	-0,035	0,015	3,6	2
0,018	-0,018	0,015	8,6	6,6
0,018	0	0,015	16,3	9
0,018	0,018	0,015	12,9	7,6
0,018	0,035	0,015	3,8	3,4
0,035	-0,035	0,015	1,4	1,6

B.1. TABLES OF EXPERIMENTAL RESULTS

0,035	-0,018	0,015	1,4	1,2
0,035	0	0,015	8,2	3
0,035	0,018	0,015	3,4	1,2
0,035	0,035	0,015	3,8	0,6
-0,035	-0,035	0,025	1,4	1,2
-0,035	-0,018	0,025	1,8	2,8
-0,035	0	0,025	3,6	3,2
-0,035	0,018	0,025	2,2	2,4
-0,035	0,035	0,025	2	2,6
-0,018	-0,035	0,025	1,4	1,2
-0,018	-0,018	0,025	8	10,5
-0,018	0	0,025	11,1	16,7
-0,018	0,018	0,025	8,4	7,6
-0,018	0,035	0,025	3	2,8
0	-0,035	0,025	2	1,6
0	-0,018	0,025	4,6	7,4
0	0	0,025	15,1	30,2
0	0,018	0,025	10,5	9,4
0	0,035	0,025	3,4	2,4
0,018	-0,035	0,025	3	2,6
0,018	-0,018	0,025	7,4	7,4
0,018	0	0,025	18,3	14,1
0,018	0,018	0,025	13,3	9,8
0,018	0,035	0,025	3	3,4
0,035	-0,035	0,025	1	1,6
0,035	-0,018	0,025	2,8	1,4
0,035	0	0,025	6	2,4
0,035	0,018	0,025	4,4	3
0,035	0,035	0,025	2,2	1,4
-0,035	-0,035	0,035	2	1,8
-0,035	-0,018	0,035	3,6	3
-0,035	0	0,035	5,6	4,4
-0,035	0,018	0,035	5	4,4
-0,035	0,035	0,035	3	2,2
-0,018	-0,035	0,035	2,2	2,4
-0,018	-0,018	0,035	11,1	11,9
-0,018	0	0,035	14,1	11,7
-0,018	0,018	0,035	8,6	12,1
-0,018	0,035	0,035	2,6	1,4

B.1. TABLES OF EXPERIMENTAL RESULTS

0	-0,035	0,035	2,8	2,4
0	-0,018	0,035	5,2	7,6
0	0	0,035	23,1	28,5
0	0,018	0,035	4,8	7
0	0,035	0,035	3,8	3,2
0,018	-0,035	0,035	1,6	1,8
0,018	-0,018	0,035	7,4	5,6
0,018	0	0,035	17,5	19,5
0,018	0,018	0,035	14,5	12,7
0,018	0,035	0,035	2,2	2,4
0,035	-0,035	0,035	1,2	2
0,035	-0,018	0,035	2	1,8
0,035	0	0,035	5,8	3,2
0,035	0,018	0,035	3,2	3,4
0,035	0,035	0,035	2	2,2
-0,035	-0,035	0,045	2,8	2,4
-0,035	-0,018	0,045	3,8	4
-0,035	0	0,045	9,4	10,1
-0,035	0,018	0,045	3	3
-0,035	0,035	0,045	3,4	3,6
-0,018	-0,035	0,045	4	2,8
-0,018	-0,018	0,045	7,2	8,4
-0,018	0	0,045	13,5	7,6
-0,018	0,018	0,045	12,5	15,3
-0,018	0,035	0,045	4	2,4
0	-0,035	0,045	2,4	2,4
0	-0,018	0,045	8,2	8,6
0	0	0,045	21,9	27,7
0	0,018	0,045	7	3,4
0	0,035	0,045	4,5	7
0,018	-0,035	0,045	3,2	3,6
0,018	-0,018	0,045	7,3	5,6
0,018	0	0,045	12	16,1
0,018	0,018	0,045	11,9	13,3
0,018	0,035	0,045	2,8	2,2
0,035	-0,035	0,045	2	1,6
0,035	-0,018	0,045	3,2	1,6
0,035	0	0,045	7,8	3,8
0,035	0,018	0,045	2,4	2,4

B.1. TABLES OF EXPERIMENTAL RESULTS

0,035	0,035	0,045	3	2,8
-0,035	-0,035	0,055	3,2	2,4
-0,035	-0,018	0,055	2,2	2,6
-0,035	0	0,055	7,6	9,6
-0,035	0,018	0,055	4,4	2
-0,035	0,035	0,055	2,2	3
-0,018	-0,035	0,055	2,8	3,6
-0,018	-0,018	0,055	3	9
-0,018	0	0,055	10,5	5,4
-0,018	0,018	0,055	11	16,3
-0,018	0,035	0,055	6,6	4,6
0	-0,035	0,055	4,6	2,2
0	-0,018	0,055	7,6	6,6
0	0	0,055	22,7	24,5
0	0,018	0,055	3,6	4,4
0	0,035	0,055	6,4	3,2
0,018	-0,035	0,055	5,2	2
0,018	-0,018	0,055	5	4,4
0,018	0	0,055	9	11,3
0,018	0,018	0,055	7,2	10,1
0,018	0,035	0,055	5,6	5
0,035	-0,035	0,055	2	2
0,035	-0,018	0,055	1,6	1,8
0,035	0	0,055	11,3	8
0,035	0,018	0,055	3,4	3,4
0,035	0,035	0,055	1,8	3
-0,035	-0,035	0,065	3,2	4
-0,035	-0,018	0,065	2,6	5,8
-0,035	0	0,065	8	8
-0,035	0,018	0,065	4,2	2
-0,035	0,035	0,065	1,8	4,6
-0,018	-0,035	0,065	2,8	4,4
-0,018	-0,018	0,065	3,2	8
-0,018	0	0,065	10,3	4
-0,018	0,018	0,065	9,6	16,7
-0,018	0,035	0,065	6,4	5,8
0	-0,035	0,065	4	2,2
0	-0,018	0,065	7,4	3,8
0	0	0,065	23,9	23,1

B.1. TABLES OF EXPERIMENTAL RESULTS

0	0,018	0,065	3,8	4,6
0	0,035	0,065	5,4	4,2
0,018	-0,035	0,065	3,8	5,6
0,018	-0,018	0,065	5,2	3,2
0,018	0	0,065	8	10,5
0,018	0,018	0,065	6,4	10,1
0,018	0,035	0,065	4,8	5,2
0,035	-0,035	0,065	1,2	2
0,035	-0,018	0,065	1,8	1,8
0,035	0	0,065	8,4	6,8
0,035	0,018	0,065	3,2	3
0,035	0,035	0,065	1,6	3,6
-0,035	-0,035	0,075	5,6	5,2
-0,035	-0,018	0,075	5,6	8,6
-0,035	0	0,075	6	9,6
-0,035	0,018	0,075	2,2	5,6
-0,035	0,035	0,075	6,6	4
-0,018	-0,035	0,075	3,2	5
-0,018	-0,018	0,075	10,5	6
-0,018	0	0,075	14,1	6,6
-0,018	0,018	0,075	5,2	11,5
-0,018	0,035	0,075	6,8	7,4
0	-0,035	0,075	2,8	4,8
0	-0,018	0,075	8,6	6
0	0	0,075	20,7	15,9
0	0,018	0,075	9	6
0	0,035	0,075	2	2,6
0,018	-0,035	0,075	6,8	5
0,018	-0,018	0,075	2	6
0,018	0	0,075	10,1	10,5
0,018	0,018	0,075	8,2	12,5
0,018	0,035	0,075	7,2	3,8
0,035	-0,035	0,075	3,4	2,4
0,035	-0,018	0,075	2,2	1,6
0,035	0	0,075	6,8	5,8
0,035	0,018	0,075	3,8	3,8
0,035	0,035	0,075	3	3,2
-0,035	-0,035	0,085	4,8	6,8
-0,035	-0,018	0,085	3	7,8

B.1. TABLES OF EXPERIMENTAL RESULTS

-0,035	0	0,085	4,8	7,2
-0,035	0,018	0,085	2	6,2
-0,035	0,035	0,085	4,6	3,6
-0,018	-0,035	0,085	3,2	4,4
-0,018	-0,018	0,085	8	3,2
-0,018	0	0,085	15,5	6,4
-0,018	0,018	0,085	7,6	11,7
-0,018	0,035	0,085	4,2	7,6
0	-0,035	0,085	1,6	4,4
0	-0,018	0,085	5,8	6,8
0	0	0,085	18,3	17,1
0	0,018	0,085	8	3
0	0,035	0,085	3	4,4
0,018	-0,035	0,085	4,8	7
0,018	-0,018	0,085	3,2	6,4
0,018	0	0,085	8	8,4
0,018	0,018	0,085	7,6	10,5
0,018	0,035	0,085	5,4	6,8
0,035	-0,035	0,085	4,2	0,8
0,035	-0,018	0,085	1	2
0,035	0	0,085	6,4	8
0,035	0,018	0,085	5,4	8,6
0,035	0,035	0,085	5	3,2

Table B.2: Results for the tests done when focusing at $F = [0.018 \ 0 \ 0.05]$ (titled x focus) and $F = [0 \ 0.018 \ 0.05]$ (titled y focus) and for the capped sphere array.

Position			Voltage (Vpp)		
x	y	z	x focus	y focus	sphere
-0,018	-0,018	0,015	8,8	6	3,14
-0,018	0	0,015	34,4	16,3	5,83
-0,018	0,018	0,015	10,3	13,3	2,01
0	-0,018	0,015	16,9	6,8	5,31
0	0	0,015	24,7	18,5	22,5
0	0,018	0,015	12,5	11,7	9
0,018	-0,018	0,015	11,7	4,6	2,8
0,018	0	0,015	30,8	16,5	2,4
0,018	0,018	0,015	11,9	9,6	2,8
-0,018	-0,018	0,025	10,7	7,2	6,8

B.1. TABLES OF EXPERIMENTAL RESULTS

-0,018	0	0,025	30,8	13,9	6,2	
-0,018	0,018	0,025	12,1	10,3	5,4	
0	-0,018	0,025	18,1	5,2	5,2	
0	0	0,025	22,9	12,5	18,1	
0	0,018	0,025	16,9	10,1	7	
0,018	-0,018	0,025	12,1	4,2	2,2	
0,018	0	0,025	23,5	14,7	4,6	
0,018	0,018	0,025	13,5	9,6	2,4	
-0,018	-0,018	0,035	12,9	7,6	5,6	
-0,018	0	0,035	22,9	11,7	6	
-0,018	0,018	0,035	6	9,2	5,4	
0	-0,018	0,035	17,1	3,8	2,8	
0	0	0,035	22,9	5,4	18,7	
0	0,018	0,035	16,5	15,3	5,2	
0,018	-0,018	0,035	12,3	4,2	4,2	
0,018	0	0,035	25,3	10,5	6,4	
0,018	0,018	0,035	20,9	8	2,2	
-0,018	-0,018	0,045	10,9	10,9	6,4	
-0,018	0	0,045	16,1	8,4	6,6	
-0,018	0,018	0,045	4,8	9,6	5,8	
0	-0,018	0,045	10,9	3	6,8	
0	0	0,045	18,5	8,4	17,7	
0	0,018	0,045	18,5	16,5	5,8	
0,018	-0,018	0,045	13,1	5,6	8	
0,018	0	0,045	21,3	5,2	9	
0,018	0,018	0,045	10,7	7,8	4	
-0,018	-0,018	0,055	6	13,1	7,6	
-0,018	0	0,055	8,8	9,2	4,4	
-0,018	0,018	0,055	8	9,6	4	
0	-0,018	0,055	10,1	5	7,6	
0	0	0,055	22,9	6,4	14,9	
0	0,018	0,055	18,1	13,3	6	
0,018	-0,018	0,055	13,7	8,2	8,4	
0,018	0	0,055	13,3	7,4	8,8	
0,018	0,018	0,055	7	9,8	4,8	
-0,018	-0,018	0,065	8	10,5	5,6	
-0,018	0	0,065	11,7	10,7	3,6	
-0,018	0,018	0,065	5,6	10,1	3,4	
0	-0,018	0,065	11,5	5,2	8,8	

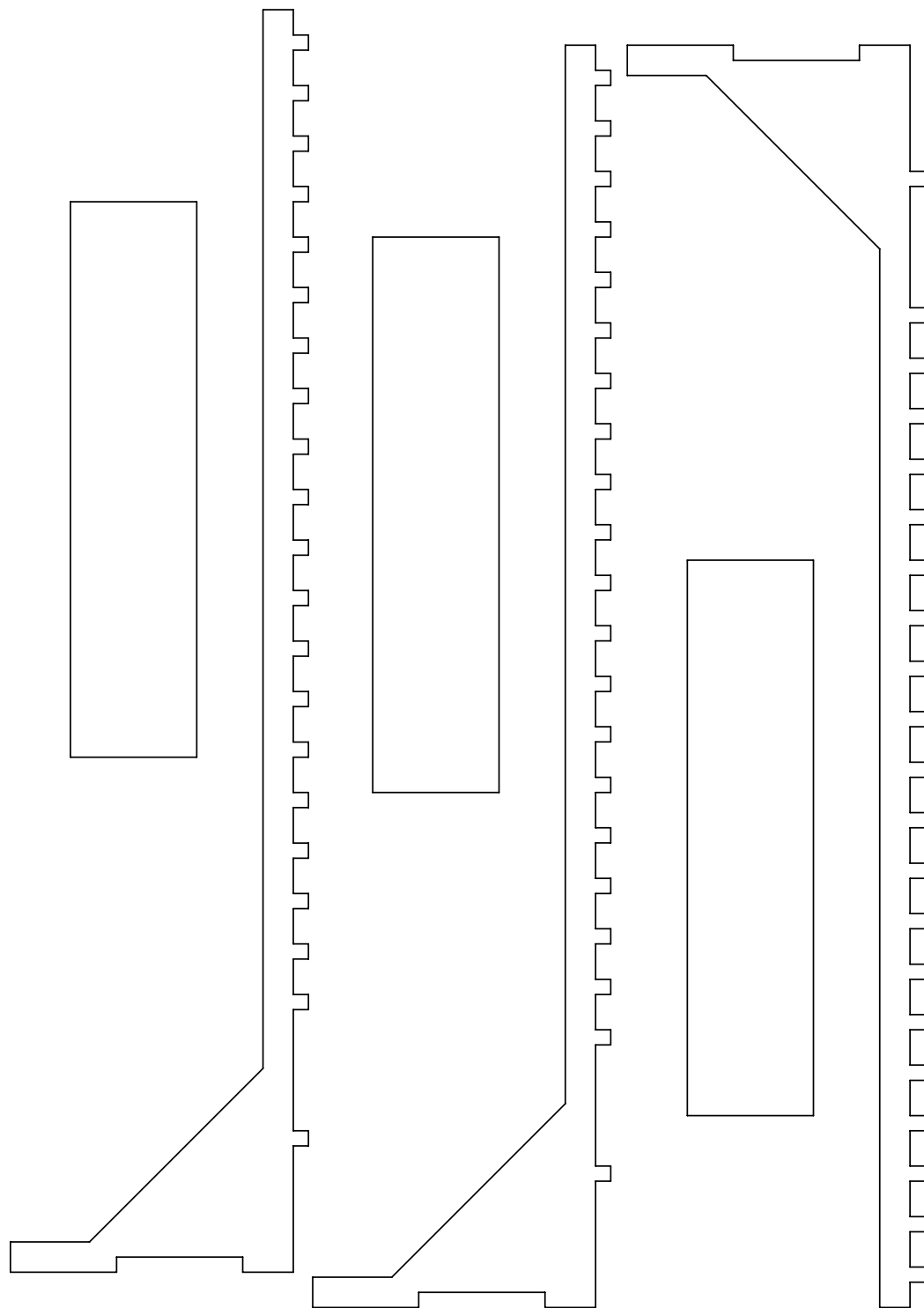
B.1. TABLES OF EXPERIMENTAL RESULTS

0	0	0,065	20,3	8,8	10,3	
0	0,018	0,065	14,7	12,3	5,6	
0,018	-0,018	0,065	12,3	7,8	11,7	
0,018	0	0,065	12,7	10,5	7,2	
0,018	0,018	0,065	9,4	7,8	5,6	
-0,018	-0,018	0,075	13,3	10,5	6	
-0,018	0	0,075	5,4	12,9	5,2	
-0,018	0,018	0,075	2,4	9,2	5,4	
0	-0,018	0,075	4,4	6	2,8	
0	0	0,075	19,3	7,6	4,8	
0	0,018	0,075	19,3	11,7	3,8	
0,018	-0,018	0,075	6	6	11,3	
0,018	0	0,075	11,1	9,6	5,6	
0,018	0,018	0,075	6,2	6	6	

Appendix C

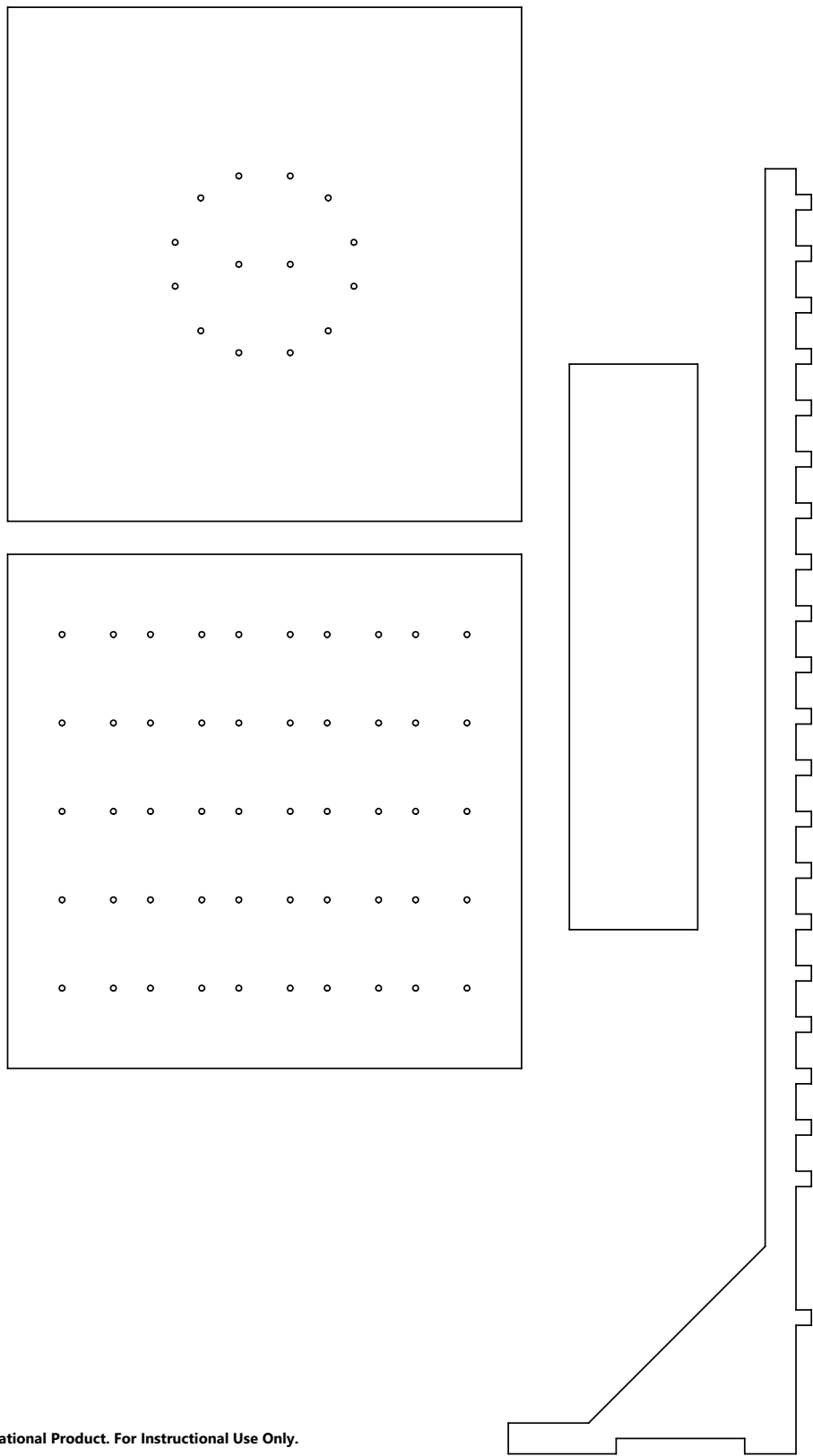
C.1 PDFs for lasercutting parts for testing stand

C.1. PDFS FOR LASERCUTTING PARTS FOR TESTING STAND



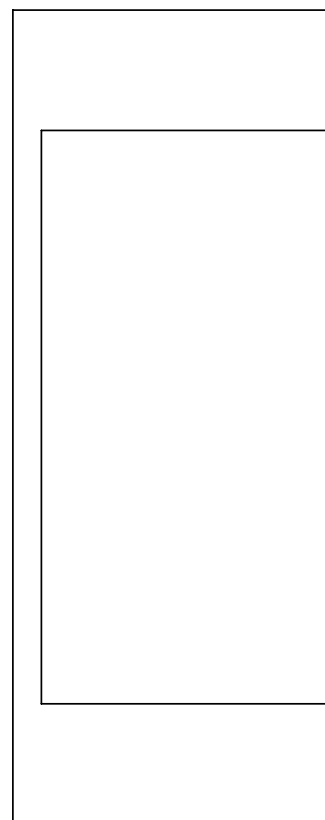
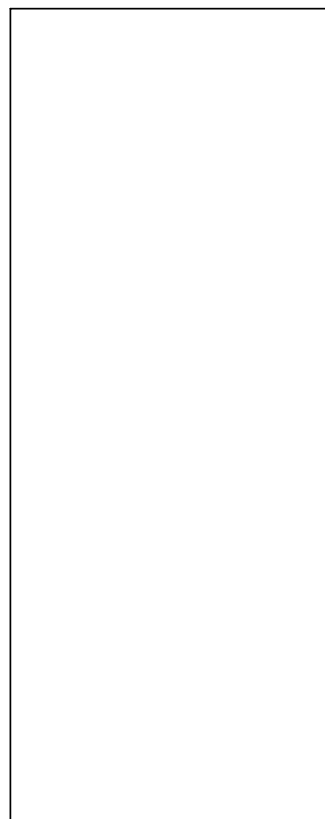
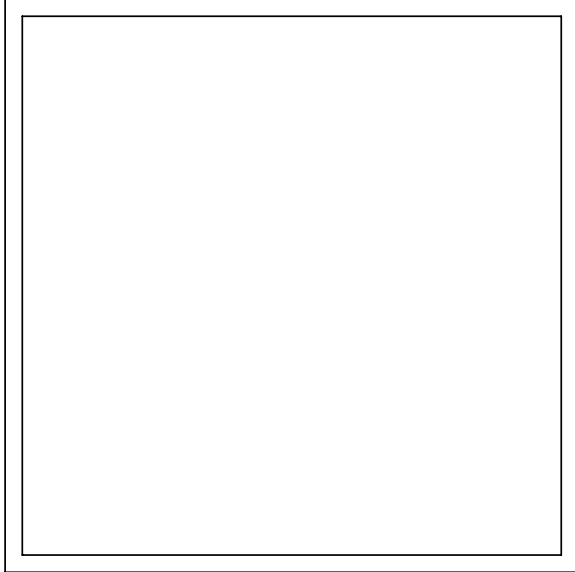
SOLIDWORKS Educational Product. For Instructional Use Only.

C.1. PDFS FOR LASERCUTTING PARTS FOR TESTING STAND



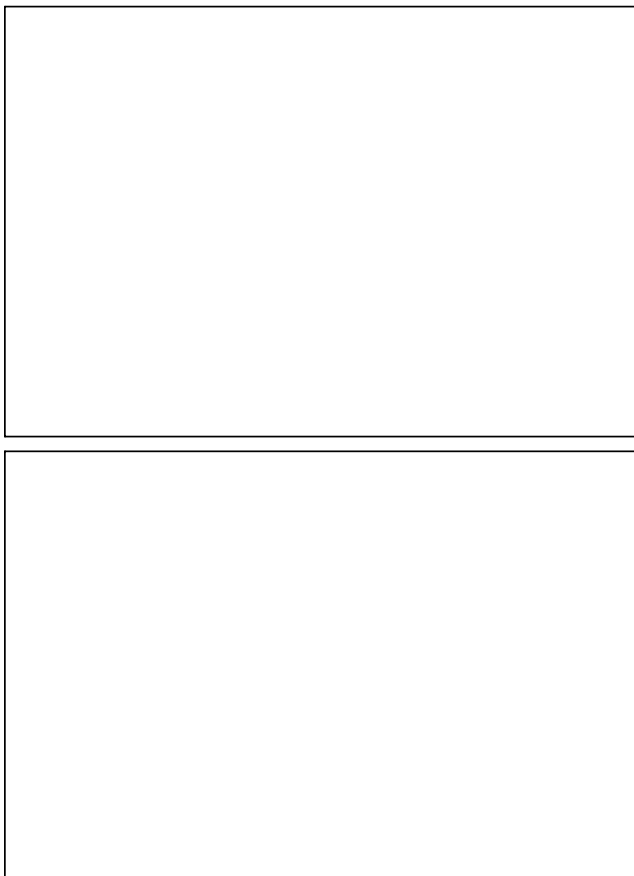
SOLIDWORKS Educational Product. For Instructional Use Only.

C.1. PDFS FOR LASERCUTTING PARTS FOR TESTING STAND

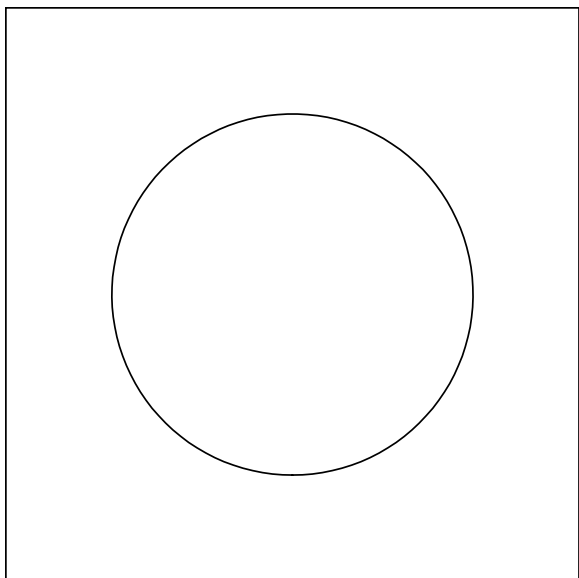


SOLIDWORKS Educational Product. For Instructional Use Only.

C.1. PDFS FOR LASERCUTTING PARTS FOR TESTING STAND



C.1. PDFS FOR LASERCUTTING PARTS FOR TESTING STAND



SOLIDWORKS Educational Product. For Instructional Use Only.